
Article:
Kim, D.W., Place, E., Chinnaiya, K. et al. (8 more authors) (2022) Single-cell analysis of early chick hypothalamic development reveals that hypothalamic cells are induced from prethalamic-like progenitors. Cell Reports, 38 (3). 110251. ISSN 2211-1247

https://doi.org/10.1016/j.celrep.2021.110251

Cell Reports

Article

Single-cell analysis of early chick hypothalamic development reveals that hypothalamic cells are induced from prethalamic-like progenitors

Graphical abstract

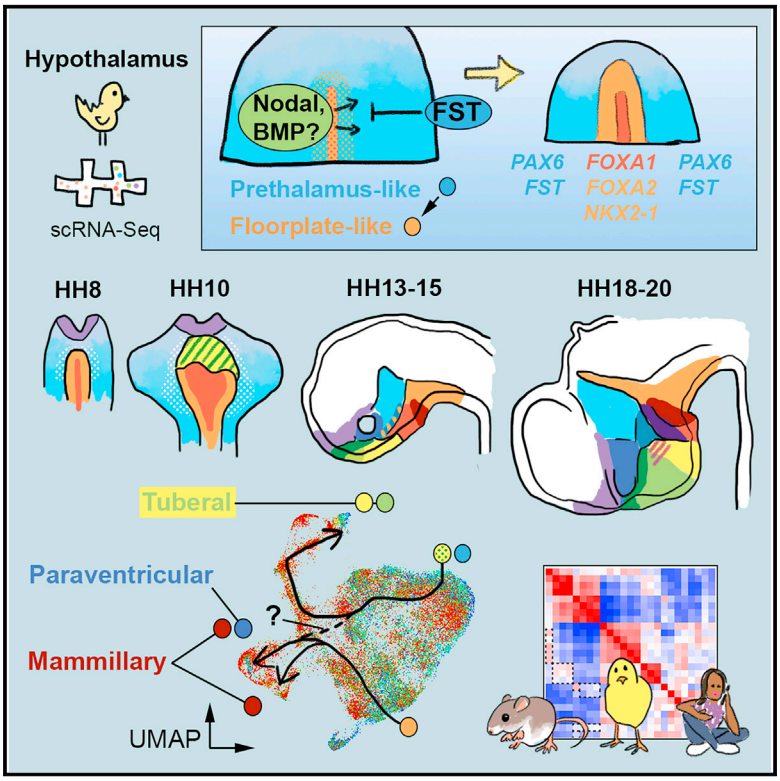

Highlights

- Early hypothalamic development was profiled in chick using scRNA-seq and HCR
- Hypothalamic cells are induced from prethalamic-like cells
- Distinct tuberal, mammillary, and paraventricular progenitor populations emerge later
- Prethalamic-like progenitor-derived follistatin inhibits hypothalamic specification

Authors

Dong Won Kim, Elsie Place, Kavitha Chinnaiya, ..., Sarah Burbridge, Marysia Placzek, Seth Blackshaw

Correspondence

m.placzek@sheffield.ac.uk (M.P.), sblack@jhmi.edu (S.B.)

In brief

Using scRNA-seq in the developing chick hypothalamus, Kim et al. identify progenitors during hypothalamic specification, regionalization, and early neurogenesis and demonstrate evolutionary conservation between major neuronal precursor subtypes. Hypothalamic progenitors are shown to arise from prethalamic-like neuroepithelial cells, and follistatin derived from these cells is found to limit hypothalamic induction.

Kim et al., 2022, Cell Reports *38*, 110251
January 18, 2022
https://doi.org/10.1016/j.celrep.2021.110251

CellPress

Cell Reports

CellPress
OPEN ACCESS

Article

Single-cell analysis of early chick hypothalamic development reveals that hypothalamic cells are induced from prethalamic-like progenitors

Dong Won Kim,[1,12] Elsie Place,[7,8,9,12] Kavitha Chinnaiya,[7,8,9,12] Elizabeth Manning,[7,8,9] Changyu Sun,[1] Weina Dai,[1] Ian Groves,[10] Kyoji Ohyama,[7,11] Sarah Burbridge,[7,8,9] Marysia Placzek,[7,8,9,*] and Seth Blackshaw[1,2,3,4,5,6,13,*]

[1]Solomon H. Snyder Department of Neuroscience, Johns Hopkins University School of Medicine, Baltimore, MD, USA
[2]Department of Psychiatry and Behavioral Science, Johns Hopkins University School of Medicine, Baltimore, MD, USA
[3]Department of Ophthalmology, Johns Hopkins University School of Medicine, Baltimore, MD, USA
[4]Department of Neurology, Johns Hopkins University School of Medicine, Baltimore, MD, USA
[5]Institute for Cell Engineering, Johns Hopkins University School of Medicine, Baltimore, MD, USA
[6]Kavli Neuroscience Discovery Institute, Johns Hopkins University School of Medicine, Baltimore, MD, USA
[7]School of Biosciences, University of Sheffield, Sheffield, UK
[8]Bateson Centre, University of Sheffield, Sheffield, UK
[9]Neuroscience Institute, University of Sheffield, Sheffield, UK
[10]School of Mathematics and Statistics, University of Sheffield, Sheffield, UK
[11]Department of Histology and Neuroanatomy, Tokyo Medical University, Tokyo, Japan
[12]These authors contributed equally
[13]Lead contact
*Correspondence: m.placzek@sheffield.ac.uk (M.P.), sblack@jhmi.edu (S.B.)
https://doi.org/10.1016/j.celrep.2021.110251

SUMMARY

The hypothalamus regulates many innate behaviors, but its development remains poorly understood. Here, we used single-cell RNA sequencing (RNA-seq) and hybridization chain reaction (HCR) to profile multiple stages of early hypothalamic development in the chick. Hypothalamic neuroepithelial cells are initially induced from prethalamic-like cells. Two distinct hypothalamic progenitor populations then emerge and give rise to tuberal and mammillary/paraventricular hypothalamic cells. At later stages, the regional organization of the chick and mouse hypothalamus is highly similar. We identify selective markers for major subdivisions of the developing chick hypothalamus and many previously uncharacterized candidate regulators of hypothalamic induction, regionalization, and neurogenesis. As proof of concept for the power of the dataset, we demonstrate that prethalamus-derived follistatin inhibits hypothalamic induction. This study clarifies the organization of the nascent hypothalamus and identifies molecular mechanisms that may control its induction and subsequent development.

INTRODUCTION

The hypothalamus regulates homeostatic physiological processes and innate behaviors via diverse neurons that lie within a patchwork of neuronally dense and sparse areas (Saper and Lowell, 2014; Swaab, 2003). Understanding hypothalamic structure and function has been challenging, but insights have been gained by studying its development, which, when disrupted, can lead to metabolic and behavioral disorders in adulthood (Bedont et al., 2015; Biran et al., 2015; Eachus et al., 2017; Moir et al., 2017; Xie and Dorsky, 2017). Characterizing mechanisms that control hypothalamic development illuminates both hypothalamic organization and function. The increased prevalence of metabolic and mood disorders underlines the importance of such knowledge.

Recent years have seen substantial progress in understanding hypothalamic development. A landmark study identified molecular markers of major hypothalamic regions in the mid-gestational (embryonic day [E]11.5–E12.5) mouse (Shimogori et al., 2010), describing tuberal and mammillary progenitor domains in the ventral hypothalamus separated from dorsal paraventricular and prethalamic progenitors by the intrahypothalamic diagonal (ID) (Figure 1A). Subsequent studies have used single-cell RNA sequencing (scRNA-seq) (Kim et al., 2020, 2021; Lee et al., 2018; Romanov et al., 2020) to comprehensively profile changes in gene expression that correlate with the specification of hypothalamic neurons. Together with traditional genetic studies (Aslanpour et al., 2020; Bedont et al., 2014; Chen et al., 2020; Kim et al., 2020; Liu et al., 2015; Lu et al., 2013; Romanov et al., 2020; Salvatierra et al., 2014), these are starting to identify molecular pathways that control the emergence of major hypothalamic neurons from defined progenitor zones. However, little is known about the earliest phases of mouse hypothalamic development.

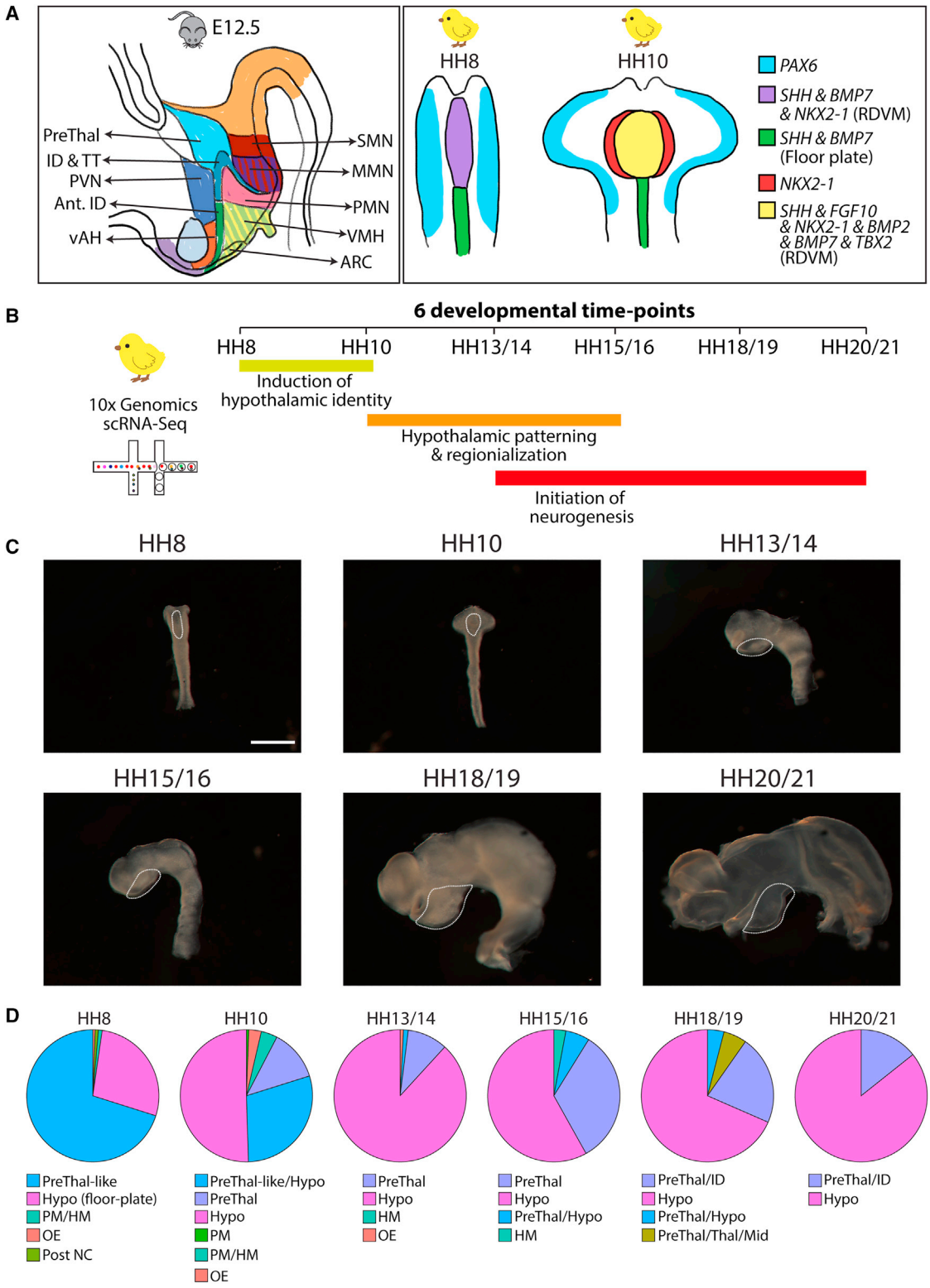

Figure 1. Generation of scRNA-seq datasets

(A) Schematics summarize current knowledge: panels show hypothalamic progenitor/early neurogenic regions in E12.5 mice and in HH8 and HH10 chicks.

(B) Schematic showing scRNA-seq experimental design. Hypothalamic tissue was isolated at six developmental timepoints between HH8 and HH20/21.

(C) Wholemount views of isolated neuroectoderm showing dissected areas (white dotted regions) at HH8, HH10, HH13/14, HH15/16, HH18/19, and HH20/21.

(legend continued on next page)

The relatively large and accessible chick embryo offers an attractive system for studying early hypothalamic development (Blackshaw et al., 2010; Burbridge et al., 2016). The earliest chick hypothalamic progenitors are floor-plate-like cells, termed rostral diencephalic ventral midline (RDVM) cells, that express *SHH*, *BMP7*, and *NKX2-1* (Figure 1A) (Dale et al., 1997, 1999; Ohyama et al., 2005). RDVM cells are induced around Hamburger–Hamilton stage 8 (HH8) through the combined action of Sonic hedgehog (SHH), Nodal, and bone morphogenetic protein (BMP) signals from prechordal mesendoderm (Dale et al., 1999; Manning et al., 2006; Ohyama et al., 2005; Patten et al., 2003; Pera and Kessel, 1997). Some RDVM cells later upregulate *TBX2*, *BMP2*, and *FGF10* in response to BMP signals (Figure 1A) (Manning et al., 2006) and generate tuberal and mammillary hypothalamic progenitors (Fu et al., 2017; Manning et al., 2006).

Here, we used scRNA-seq to profile gene expression in the chick hypothalamus at six stages covering hypothalamic induction, regionalization, and early neurogenesis. We identified both known and novel markers that, when validated with multiplexed hybridization chain reaction (HCR) analysis, allowed us to define and link major spatial domains at each stage. At HH8, the earliest stage profiled, the hypothalamus is a heterogeneous population of midline neuroepithelial cells that is located adjacent to diencephalic prethalamic-like progenitors. Hypothalamic progenitors undergo dramatic expansion by HH10 and by HH13–16 are organized into distinct mammillary and tuberal progenitor subsets. By HH18–HH21, tuberal, mammillary, and paraventricular region-specific progenitors express markers that resemble those seen in mid-gestational mouse and human.

Using RNA velocity to infer cell lineage relationships (La Manno et al., 2018), we show that hypothalamic cells emerge from prethalamic-like cells and validate this using an *ex vivo* culture system. Through gain- and loss-of-function studies, we demonstrate that the newly identified prethalamic-like progenitor marker follistatin inhibits hypothalamic induction.

Our study provides a molecular roadmap for early hypothalamic development at unprecedented spatial and temporal resolutions, confirms the extensive evolutionary conservation of hypothalamic organization and development, reveals unexpected molecular homologies among developing hypothalamic regions, and identifies a new factor controlling hypothalamic induction.

RESULTS

scRNA-seq analysis of early chick hypothalamic development

To profile gene expression during early chick hypothalamic development, we analyzed six timepoints covering hypothalamic induction (HH8: 3–5 somites), patterning and regionalization (HH10: 9–11 somites, HH13/14, and HH15/16), and early neurogenesis (HH13/14, HH15/16, HH18/19, and HH20/21) (Figure 1B). Hypothalamic tissue was isolated using anatomical landmarks (Figure 1C). Between 4,000 and 20,000 cells were profiled at each stage (76,000 cells in total), and UMAP datasets were generated (Figures S1A and S1B). Minimal contamination from telencephalic (*FOXG1*-positive) or non-neuronal cells was seen (Figures 1D, S2A, S2K, S4B, and S4E). Prethalamic-like cells (*PAX6*-positive) (see below) were the main cell type detected at HH8, with hypothalamic cells (*SHH*-positive) being less common (Figure 1D). From HH8 through HH20/21, there were progressively fewer prethalamic-like progenitors (*PAX6*) and more hypothalamic cells (*SHH*/*NKX2-1*) (Figure 1D).

Specification of hypothalamic identity

HH8 scRNA-seq datasets showed that clusters $C1^{HH8}$, $C2^{HH8}$, $C3^{HH8}$, and $C5^{HH8}$ express floor plate/RDVM markers (*SHH*/*FOXA1*/*FOXA2*/*CHRD*, low *NKX2-1*/*BMP7*) (Figures 2A and 2B). They also selectively express genes not previously seen in RDVM cells, including hypothalamic-enriched transcription factors (*NKX2-4*/*DBX1*/*SIX6*/*VAX1*), signaling pathway components (*BMP2*), hypothalamic hormones (*SST*/*POMC*), and other categories of genes (*OLFML3*/*CA2*/*NOV*) (Figure S2A; Table S1). $C1^{HH8}$, $C2^{HH8}$, $C3^{HH8}$, and $C5^{HH8}$ therefore represent hypothalamic floor-plate-like clusters.

Clusters $C8^{HH8}$–$C10^{HH8}$, in contrast, consist of cells that express markers of prethalamic progenitors and maturing prethalamic cells (*PAX6*/*DLX2*/*OLIG2*/*MEIS2*/*SP8*) (Figure 2B) (Bailey et al., 2006; Ferran et al., 2008; Larsen et al., 2001; Kim et al., 2020; Shimogori et al., 2010). Individual clusters in this group were distinguished by different expression levels of cell-cycle regulators (*CENPF*) and sex-chromosome-specific genes (*WPKCI-7*) (Figure S2A). Follistatin (*FST*) and *FGF18* also marked these clusters (Figures 2B and S2A). Since markers of the eye field (*RAX*) (Ohuchi et al., 1999) and the prethalamic/hypothalamic border during neurogenesis (*NKX2-2*) (Ohyama et al., 2005) are also detected in clusters $C8^{HH8}$–$C10^{HH8}$, we refer to $C8^{HH8}$–$C10^{HH8}$ as prethalamic-like clusters.

Three separate clusters that contained few cells ($C4^{HH8}$, $C6^{HH8}$, and $C7^{HH8}$) correspond to prechordal mesendoderm/mesenchyme, neural crest, and oral ectoderm based on the expression of *TWIST1*, *HOXB2*, and *DLX5*, respectively (Figure 2A; Table S1). Most HH8 cells thus fall into 2 major cluster types: hypothalamic floor-plate-like and prethalamic-like. When subjected to RNA velocity analysis, a bioinformatics method that predicts the future state of individual cells over a timescale of hours (La Manno et al., 2018), the HH8 dataset showed trajectories that extend from prethalamic-like to floor-plate-like hypothalamic clusters (Figure 2C).

HH8 scRNA-seq and velocity analyses therefore indicate that early hypothalamic cells are heterogeneous and likely arise from prethalamic-like cells. To validate this, we used *in situ* HCR. This revealed heterogeneity among early hypothalamic cells along the medio-lateral axis. Some hypothalamic marker genes

(D) Pie charts showing the distribution of prethalamic/hypothalamic progenitor cells and contaminating tissues across the 6 developmental timepoints.
Scale bar in (C), 800 μm. Ant. ID, Anterior ID; ARC, arcuate nucleus; HM, head mesoderm/mesenchyme; Hypo, hypothalamus; ID, intrahypothalamic diagonal; Mid, midbrain; MMN, mammillary nucleus; OE, oral ectoderm; PM, prechordal mesoderm; Post NC, posterior neural crest; PreThal-like, prethalamus-like progenitors; PreThal, prethalamus; PVN, paraventricular nucleus; PMN, premammillary nucleus; RDVM, rostral diencephalic ventral midline; SMN, supramammillary nucleus; Thal, thalamus; TT, tuberomammillary terminal; vAH, ventral-anterior hypothalamus; VMH, ventromedial hypothalamus.

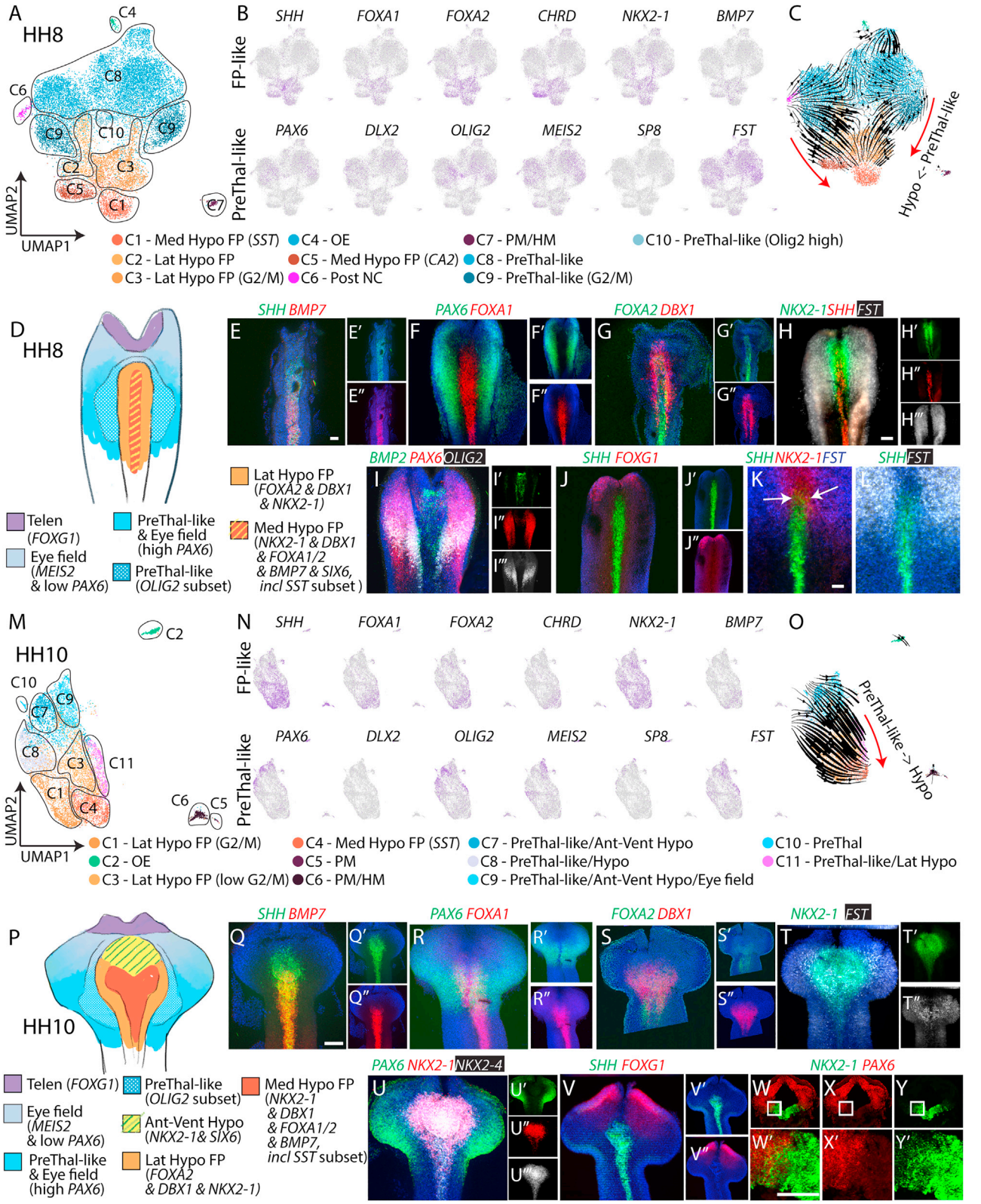

(legend on next page)

(*SHH*/*BMP7*/*CA2*/*SIX6*/*SST*) are expressed narrowly (Figures 2E and S2B–S2D), others (*FOXA2)* more broadly (Figures 2F and 2G), and a third set (*DBX1*/*NKX2-1*/*BMP2*) more broadly still (Figures 2G–2I, S2B, and S2E). There is also heterogeneity along the anteroposterior (A-P) axis. *DBX1*/*NKX2-1*/*BMP2* taper from a broad anterior domain to two narrow parallel posterior domains. In contrast, *CHRD*/*FOXA2* are strongly expressed in the posterior midline and expressed more weakly anteriorly. These analyses allow progenitor clusters identified using scRNA-seq to be matched to spatial domains of gene expression and show that even at HH8, the hypothalamus is heterogeneous (Figures 2A and 2D). Notably, though, this heterogeneity does not clearly prefigure future spatial organization: *SIX6*/*SST*/*DBX1*/*NKX2-2* show extensive overlap along the A-P axis, although each will later mark distinct progenitor subsets.

HCR also supports the idea that the hypothalamus emerges from prethalamic-like cells. At the HH8 3–4 somite stage, early hypothalamic cells are surrounded by prethalamic-like progenitor cells (*FST*/*PAX6*/*OLIG2*/*NKX2-2)* and are aligned with cells that express *RAX* (Figures 2H–2L and S2E–S2F). Hypothalamic and prethalamic markers overlap (Figures 2K, 2L, and 2W–2Y′). The early developing hypothalamus is thus surrounded by prethalamic-like cells that also co-express genes enriched in the eye field (*RAX*). Only anterior-most hypothalamic cells lie adjacent to *FOXG1*-positive telencephalic progenitors. By the HH8 5-somite stage, prethalamic-like cells surrounding the hypothalamus are regionalized along the A-P axis, characterized by opposing gradients of *MEIS2* (high anteriorly and in the eye field) and *PAX6*/*OLIG2*/*SP8* (high posteriorly) (Figures S2I and S2J).

The HH10 scRNA-seq dataset revealed similar cluster types to those found at HH8 (a mix of prethalamic and hypothalamic clusters), but most cells are now found in hypothalamic clusters. Cluster $C4^{HH10}$ is a hypothalamic floor-plate-like cluster defined by the expression of many of the same genes as at HH8 (*SHH*/*FOXA1*/*FOXA2*/*CHRD*/*SST*) (Figures 2M, 2N, and S2K). Clusters $C1^{HH10}$ and $C3^{HH10}$ express the same hypothalamic floor-plate-like genes as cluster $C4^{HH10}$ but also express hypothalamic progenitor markers (*NKX2-1*, *NKX2-4*, *BMP2*, and *DBX1*) (Figures 2M, 2N, and S2K). Clusters $C7^{HH10}$–$C11^{HH10}$ contain cells that express prethalamic-like markers (*PAX6*/*OLIG2*/*SP8*/*FST*), but $C8^{HH10}$ and $C9^{HH10}$ also express hypothalamic progenitor markers (*NKX2-1*/*NKX2-4*/*BMP2*), including *NKX2-2*/*SIX6*/*VAX* (Figures 2M, 2N, and S2K; Table S2). *FGF10* is now weakly expressed in all hypothalamic clusters (Figures S2A and S2K). RNA velocity again reveals trajectories extending from prethalamic-like to hypothalamic clusters (Figure 2O), although we note a lone trajectory arising from $C9^{HH10}$. Its origin, in *SIX6*/*MEIS2* progenitors, suggests that these may be eye field cells (Marcos et al., 2015). Hypothalamic progenitor cells thus continue to be generated from prethalamic-like progenitors at HH10 and proportionally increase relative to prethalamic-like progenitors from HH8 to HH10.

Multiplex HCR shows three marked changes in gene expression in the 4–5 h period between HH8 and HH10. First, new genes are upregulated—as exemplified by *FGF10*, which broadly co-localizes with *SHH*. Second, the hypothalamus expands laterally: *SHH*/*FOXA2*/*DBX1*/*NKX2-1*/*NKX2-4*/*BMP2* expand more than *SST*/*FOXA1*/*BMP7*. Thus, there is an increasingly clear distinction between medial and lateral hypothalamic floor-plate-like domains (Figures 2L, 2Q–2V, and S2N–S2R). Third, *SIX6* is now detected anterior to *FOXA1*/*FOXA2*/*DBX1*/*SST*/*BMP7* when they are co-aligned at HH8 (Figures S2M–S2O, and 2Q–2S). At neurogenic stages, *SIX6* is expressed in the optic midline and the tuberal hypothalamus, suggesting that tuberal progenitors are emerging by HH10. *FST*/*SP8*/*PAX6* expression remains strong in lateral-most regions that include prethalamic-like and optic area cells (Figures 2T, 2U, and S3) (Garcia-Lopez et al., 2009), and HCR shows continued overlap of prethalamic and hypothalamic markers (Figures 2W–2Y′, S2I, S2J, and S3). In summary, by HH10, hypothalamic progenitor cells expand considerably, and a distinct tuberal progenitor domain emerges (Figures 2M and 2P).

Further hypothalamic regionalization

Separate analysis of scRNA-seq data from HH13/14 and HH15/16 demonstrated a very similar pattern of clusters (Figure S4), and these datasets were aggregated for further analysis. Analysis of aggregated data shows that hypothalamic organization has advanced by HH13–16, with regional identity becoming obvious and the first neurons generated (Figure 3A). Four clusters ($C3^{HH13\text{-}16}$, $C4^{HH13\text{-}16}$, $C5^{HH13\text{-}16}$, and $C8^{HH13\text{-}16}$) consist of progenitor cells. $C4^{HH13\text{-}16}$ contains the most cells and is composed of prethalamic-like progenitor cells (*PAX6*/*OLIG2*/*SP8*), hypothalamic cells (*NKX2-1*), and hypothalamic border-like cells (*NKX2-2*) (Figures 3B and S4H). The remaining three progenitor clusters ($C3^{HH13\text{-}16}$, $C5^{HH13\text{-}16}$, and $C8^{HH13\text{-}16}$) consist of hypothalamic progenitor cells (*NKX2-1*/*NKX2-4*/*SHH*) (Figure 3B). As at HH8 and HH10, one of these ($C3^{HH13\text{-}16}$) is distinguished by the expression of floor-plate-like markers (*FOXA1*/*FOXA2*/*CHRD*) but also expresses genes enriched in the mammillary/supramammillary hypothalamus (*PITX2*/*NKX6-2*/*DBX1*) (Figures 3B and S4H). Adjacent to cluster $C3^{HH13\text{-}16}$ is a

Figure 2. Specification of hypothalamic identity at HH8–HH10

(A–C and M–O) UMAP plots showing: HH8 (A) and HH10 (M) clusters and annotations; HH8 (B) and HH10 (N) representative gene expression profiles demarcating hypothalamic floor-plate-like and prethalamic-like clusters; and HH8 (C) and HH10 (O) scRNA-seq trajectories obtained from RNA velocity.

(D and P) Schematic diagrams (ventral views) showing prethalamic and hypothalamic regions relative to other progenitor domains at HH8 (D) and HH10 (P), color-coded to match UMAP plots.

(E–L and Q–V″) Maximum intensity projections showing ventral views after wholemount *in situ* HCR on isolated neuroectoderm at HH8 (E–L) or HH10 (Q–V) for combinations of transcription factors and ligands (n = 5–15 each). Embryos shown in (H) and (K) are 5- and 3 somites, respectively: in each, *NKX2-1* and *FST* show similar posterior boundaries along the A-P axis. *NKX2-1*/*FST* co-localize (R = 0.41, analysis conducted on the entire field of view shown in K).

(W and Y) Transverse sections after *in situ* HCR to detect *NKX2-1*/*PAX6*. High magnification views of boxed regions shown in (W) and (Y) used as regions of interest (ROIs) for co-localization (R = 0.23).

Scale bars, 100 μm. Ant, anterior; Dor, dorsal; FP, floor plate; Lat, lateral, Med, medial; NC, neural crest; Post, posterior; Telen, telencephalon. Other abbreviations as per Figure 1.

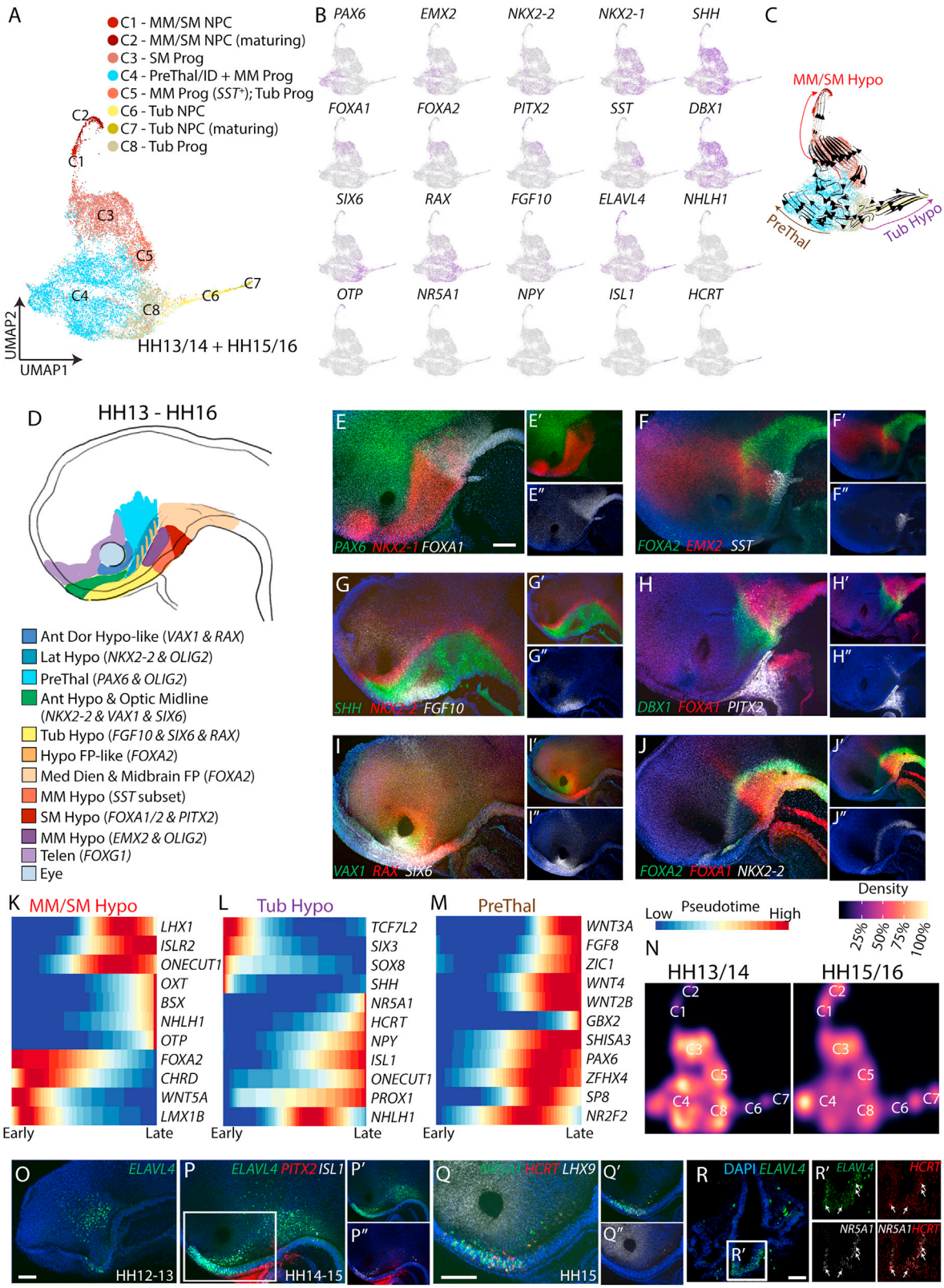

(legend on next page)

SST-expressing progenitor cluster ($C5^{HH13-16}$) (Figure 3B). RNA velocity indicates that a subset of C5 progenitors gives rise to $C3^{HH13-16}$ progenitors (Figure 3C). A fourth progenitor cluster ($C8^{HH13-16}$), which expresses *SIX6*, *RAX*, and *FGF10* (Figure 3B; Table S3),represents tuberal hypothalamic progenitors. Therefore, both tuberal and mammillary/supramammillary progenitor domains are distinct by HH13–HH16.

Multiplex HCR on hemi-dissected heads and sagittal sections reveals that the four progenitor clusters map to spatially resolving progenitor domains at HH13–HH16. The prethalamus (*PAX6*/*EMX2*) lies dorsal and posterior to the *NKX2-1*/*SHH*-positive hypothalamus (Figures 3E–3G). Within the hypothalamus, *EMX2*/*DBX1* and *SIX6* distinguish mammillary/supramammillary and tuberal progenitors, respectively (Figures 3F, 3H, 3I, and S5A). Mammillary and supramammillary domains can be distinguished by *SST* and *FOXA2*, which are expressed in adjacent domains (Figure 3F). The overlap of *FOXA1*/*FOXA2* and *PITX2* (Figures 3F, 3H, 3J, and S5B) suggests that this domain is the supramammillary hypothalamus, while the *SST*-positive domain (Figure 3F) is a previously unidentified mammillary domain. *EMX2*/*OLIG2*-positive mammillary cells lie dorsal to the *SST*-positive progenitors (Figures 3F and S5C). As in mouse and zebrafish, *NKX2-2* expression marks an arching border around the hypothalamus (Figure 3G). Anterior-most *NKX2-2*-positive cells overlap *VAX*/*RAX* and separate the *FOXG1*-positive telencephalon from *RAX*/*SHH*/*FGF10* tuberal progenitors (Figures 3G,3I,3J, S5A, and S5B). Posterior *NKX2-2*-positive cells, by contrast, separate the *PAX6*-positive prethalamus and the *NKX2-1*-positive hypothalamus and overlap with *EMX2* and *FOXA2* (Figures 3E–3G). Comparison with the HH10 HCR (Figure 2) suggests how these progenitor domains arise (compare schematics in Figures 2P and 3D).

Initiation of neurogenesis

In addition to hypothalamic progenitor clusters, we observe hypothalamic neurogenic clusters (*ELAVL4*/*NHLH1*-positive), which are apparent as two distinct neurogenic trajectories (C1/$C2^{HH13-16}$ and C6/$C7^{HH13-16}$) (Figures 3A and 3B). RNA velocity indicates that cluster $C3^{HH13-16}$ gives rise to $C1^{HH13-16}$ and $C2^{HH13-16}$ (Figure 3C). These cells represent mammillary and/or paraventricular cells, as they express the well-characterized markers *SIM1* (Caqueret et al., 2005) and *CALB2* (Shimogori et al., 2010) (Figure S4H; Table S3). Cells at the distal tip of this trajectory express the transcription factors *NHLH1* and *OTP* (Figure 3B) and the neurohormones *AVP* and *OXT* (Figure S4H; Table S3), all of which are later expressed in the paraventricular nucleus (Xu et al., 2020). This implies that neuronal precursors in this trajectory give rise to both mammillary and paraventricular neurons. Pseudotime analysis shows a progressive decrease in expression of floor-plate-like markers (*FOXA2*/*CHRD*) and a corresponding increase in mammillary markers (*LHX1*/*ISLR2*/*ONECUT1)* (Figure 3K) (Marion et al., 2005; Shimogori et al., 2010).

The second neurogenic differentiation trajectory arises from cluster $C8^{HH13-16}$ (Figures 3A and 3C). In keeping with the identification of $C8^{HH13-16}$ as a tuberal progenitor cluster, $C6^{HH13-16}$ and $C7^{HH13-16}$ cells express genes that mark tuberal hypothalamic neurons, including *ISL1* (Table S3), *NR5A1*, and *NPY* (Figure 3B) (Shimogori et al., 2010). We also note low levels of *OTP* in clusters $C6^{HH13-16}$ and $C7^{HH13-16}$, in line with reports that *OTP* is detected in zebrafish and mouse tuberal progenitors (Muthu et al., 2016; Wang and Lufkin, 2000). Unexpectedly, some C6/$C7^{HH13-16}$ cells express the arousal-promoting neuropeptide *HCRT* (Figure 3B), which is selectively found in the lateral hypothalamic area in mice. In mouse and zebrafish, *LHX9* is expressed in *HCRT*-positive neurons and activates *HCRT* expression (Dalal et al., 2013; Liu et al., 2015), but *LHX9* expression is not detected in $C7^{HH13-16}$ *HCRT* cells (Table S3). The functional significance of this species-specific difference is unclear.

Pseudotime analysis confirms upregulation of *NR5A1*/*ISL1*/*NPY*/*HCRT* as tuberal progenitors generate neurons, as well as upregulation of the premammillary-enriched homeodomain factor *PROX1* (Kim et al., 2020; Shimogori et al., 2010), transient expression of *NHLH1*, and a rapid reduction in *SIX3*/*SOX8*/*SHH* expression (Figure 3L). UMAP plots show an increase in neurogenic cells ($C1^{HH13-16}$, $C2^{HH13-16}$, $C6^{HH13-16}$, and $C7^{HH13-16}$) and a decrease in hypothalamic progenitor cells ($C3^{HH13-16}$, $C5^{HH13-16}$, and $C8^{HH13-16}$) from HH13 to HH16 (Figure 3N). RNA velocity no longer suggests a trajectory connecting prethalamic-like with tuberal and mammillary progenitor clusters, indicating that prethalamic-like cluster cells now generate only prethalamic cell types (Figure 3C). As they do so, they progressively upregulate *PAX6*/*FGF8*/*GBX2* while transiently expressing *NR2F2* (Figure 3M).

Multiplex HCR confirms the results of scRNA-seq. Small patches of *ELAVL4*-positive neural precursors are seen from HH13 in two spatially distinct domains (Figures 3O and 3P). Anterior *ELAVL4*-expressing cells lie in the *SIX6*/*NKX2-1*-positive

Figure 3. Regionalization of the hypothalamus and initiation of neurogenesis

(A–C) UMAP plots showing (A) HH13–HH16 integrated clusters and annotations, (B) distribution of representative genes demarcating hypothalamic progenitor and neurogenic regions, and (C) scRNA-seq mammillary/supramammillary, tuberal, and prethalamic trajectories obtained from RNA velocity.

(D) Schematic sideview showing developing hypothalamic regions and adjacent domains; colored regions approximate their counterparts in Figures 2D and 2P.

(E–J″) Maximum intensity projections of hemi-dissected HH14–HH15 heads after wholemount *in situ* HCR triple labeling with combinations of regional progenitor markers. Anterior to the left.

(K–M) Pseudotime analysis of mammillary/suprammillary hypothalamus (K), tuberal hypothalamus (L), and prethalamus (M).

(N) UMAP plot showing distribution of HH13/14 and HH15/16 cells across clusters.

(O–Q) Maximum intensity projections of hemi-dissected HH13–HH15 heads after wholemount *in situ* HCR to show patterns of neurogenesis and onset of tuberal-specific neural precursor cells.

(R and R′) Transverse section through the tuberal hypothalamus and optic stalk after triple *in situ* HCR for *ELAVL4*, *NR5A1*, and *HCRT* (n = 5–8 embryos each for E–I and O–R).

Scale bars, 100 μm. Dien, diencephalon; MM, mammillary; NPC, neuronal precursor cells; OM, optic midline; Prog, progenitors; SM, supramammillary; Tub, tuberal. Other abbreviations as per Figures 1 and 2.

tuberal progenitor domain (compare Figures S5A, S5B, and S5D). Posterior *ELAVL4*-positive cells within the mammillary domain co-express *PITX2* (Figure 3P). In keeping with the scRNA-seq, we detect a substantial increase in neurogenesis from HH13, and by HH14–HH15, many more *ELAVL4*-expressing cells are seen, many of which also express *ISL1* (Figure 3P) and *NR5A1* (Figures 3Q and 3R). *HCRT* expression is restricted to a subset of *NR5A1*-positive cells (Figures 3Q and 3R). Cell clusters identified by scRNA-seq thus reflect distinct progenitor domains and postmitotic neural precursor cells within the tuberal and mamillary domains.

Both scRNA-seq and HCR data confirm and extend earlier studies to show that hypothalamic induction, patterning, and regionalization occur from HH8–HH16. Previous studies have focused on how signaling ligands control patterning and regionalization of the developing hypothalamus. Our scRNA-seq studies reveal dynamic expressions of such key signaling ligands between HH8 and HH13 and their likely receptors. This analysis also identifies other receptor-ligand pairs that have not yet been linked to control of hypothalamic development (Figures S6A–S6D).

Finalizing the overall plan of hypothalamic organization

scRNA-seq at HH18/19 and HH20/21 indicates that by these stages, the overall spatial organization of the developing chick hypothalamus is complete. The same progenitor markers (prethalamic-like/ID [*PAX6*/*OLIG2*/*NKX2-2*], tuberal [*RAX*/*SIX6*/*FGF10*], mammillary/supramammillary/floor-plate-like [*FOXA1*/*FOXA2*/*PITX2*/*SST*]) and neurogenic markers (tuberal [*NR5A1*/*POMC*] and mammillary/paraventricular nucleus [PVN] [*SIM1*/*OTP*/*AVP*]) are seen as at HH13/16 (Figure S4), but numerous additional molecular markers are detected in discrete HH18/19 and HH20/21 clusters (Figure S7; Tables S4 and S5). Some of these are known to specifically label major spatial subdivisions of the developing mouse hypothalamus (Shimogori et al., 2010). For instance, *DLX1* expression is now detected in the ID (Tables S4 and S5). Further, neuronal-subtype-specific markers that were weakly detected at HH13–HH16, such as *AVP*/*POMC*, are now robustly expressed (Figure S7).

Using molecular markers analyzed in the E11.5 mouse (Shimogori et al., 2010), we performed multiplex HCR analysis at HH18 and HH20. This revealed that as early as HH18, the regional organization of the chick hypothalamus is remarkably similar to that of the E11.5 mouse (Shimogori et al., 2010) (Figure 4A). The prethalamus, which can now be delineated through *DLX1*/*OLIG2*, is located dorsally and posteriorly to the hypothalamus (Figure 4B). The ID and the ventrally extending tuberomammillary terminal (TT) are contiguous with and molecularly similar to the prethalamus, and both express *DLX1* (Figures 4B and 4C). The ID, TT, and prethalamus can, nonetheless, be distinguished through the expression of *NKX2-2* in only the ID and the expression of *PAX6* in only the prethalamus (Figures 3C and 3E–3G).

Adjacent and posterior-ventral to the TT, *EMX2* and *FOXA1*/*PITX2* define the mammillary hypothalamus and supramammillary hypothalamus, respectively (Figures 4D, 4E, 4H, and 4I). At this stage, the largest hypothalamic territory is the developing tuberal region, lying anteriorly to the mammillary region, ventrally to the ID, and dorsally to Rathke's pouch and including the *PROX1*+ premammillary region in the crook of the ID and TT (Figure 4E). The posterior limits of the prethalamus and hypothalamus are defined by the *SHH*-positive ZLI dorsally (Figure 4F) and by the *ARX*-positive di/mesencephalic floor plate ventrally (Figure 4K). *ARX* also marks the prethalamus, ID, and TT, as in mouse (Figure 4K).

Finally, the anterior-dorsal paraventricular region is marked by *SIM1* and *VAX1* expression (Figures 4B and 4J). The *SIM1*-positive paraventricular territory is separated from a *SIM1*-positive mammillary territory by the ID and TT (Figure 4B). Transverse sections (planes shown in Figure 4A) show that *SIM1* is in the mantle zone and, in paraventricular regions, is adjacent to *VAX*-positive cells. Hypothalamic *SIM1*-positive cells are contiguous with those found in the *FOXG1*-positive telencephalon (Figures 4L and 4M).

Distinct tuberal and mammillary subregions can be distinguished. The anterior subdivision of the tuberal region is characterized by higher levels of *VAX* and *SIX6,* while the posterior subdivision, dorsal to Rathke's pouch, is characterized by higher *RAX* (Figure 4J). Transverse sections (planes shown in Figure 4A) show that neuronal precursors expressing markers of the ventromedial and arcuate nuclei (*NR5A1* and *POMC*, respectively) occupy the mantle zone of the tuberal domain but are as yet intermingled (Figures 4O–4Q).

Likewise, although the posterior hypothalamus is broadly divided into *FOXA1*/*PITX2*-positive supramammillary and *EMX2*-positive mammillary regions, subdomains exist within these, that can be distiguished through differential expression of these markers and of *SST*, *SIM1*, *OLIG2*, and *FOXA2* (Figures 4A–4D, 4H, 4I, and 4K). *DBX1* partially overlaps with both *EMX2*/*OLIG2*-positive and *FOXA1*/*PITX2*-positive regions (Figure 4I). Transverse sections show that *SIM1*- and *DLX1*-positive cells are intermingled in a mantle zone located between the mammillary and dorsal TT regions (Figure 4N), while *SIM1*/*OTP*-positive neuronal precursors are found in the mantle zone in both *EMX2*-positive mammillary and *PITX2*-positive supramammillary domains (Figures 4R–4U). By HH18/19, hypothalamic regionalization is complete, and postmitotic neuronal precursors are abundant in the tuberal and mammillary hypothalamus.

Gene networks controlling hypothalamic regionalization and neurogenesis

We next sought to identify gene networks that control hypothalamic regionalization and neurogenesis. Since our samples did not profile substantial numbers of prethalamic progenitors from HH13/14 and HH15/16, we removed maturing prethalamic/ID cells, along with a small number of other non-hypothalamic cell types, then computationally aggregated all scRNA-seq data from HH8, HH10, HH13/14, HH15/16, HH18/19, and HH20/21 using UMAP analysis. This revealed a continuous distribution across the time points, which we interrogated using RNA velocity and pseudotime analysis. From HH8 onwards, we observed two major progenitor populations (Figure 5A; Table S6). Cluster $C0^{HH8\text{-}21}$ corresponded to *FOXA1*/*FOXA2*/*PITX2*-positive floor-plate-like/mammillary progenitors, and cluster $C1^{HH8\text{-}21}$ corresponded to a mixture of *RAX*/*SIX6*-positive tuberal and *FST*/*PAX6*-positive prethalamic-like progenitors (Figures 5A–5C). RNA velocity plots indicate that trajectories from both progenitor

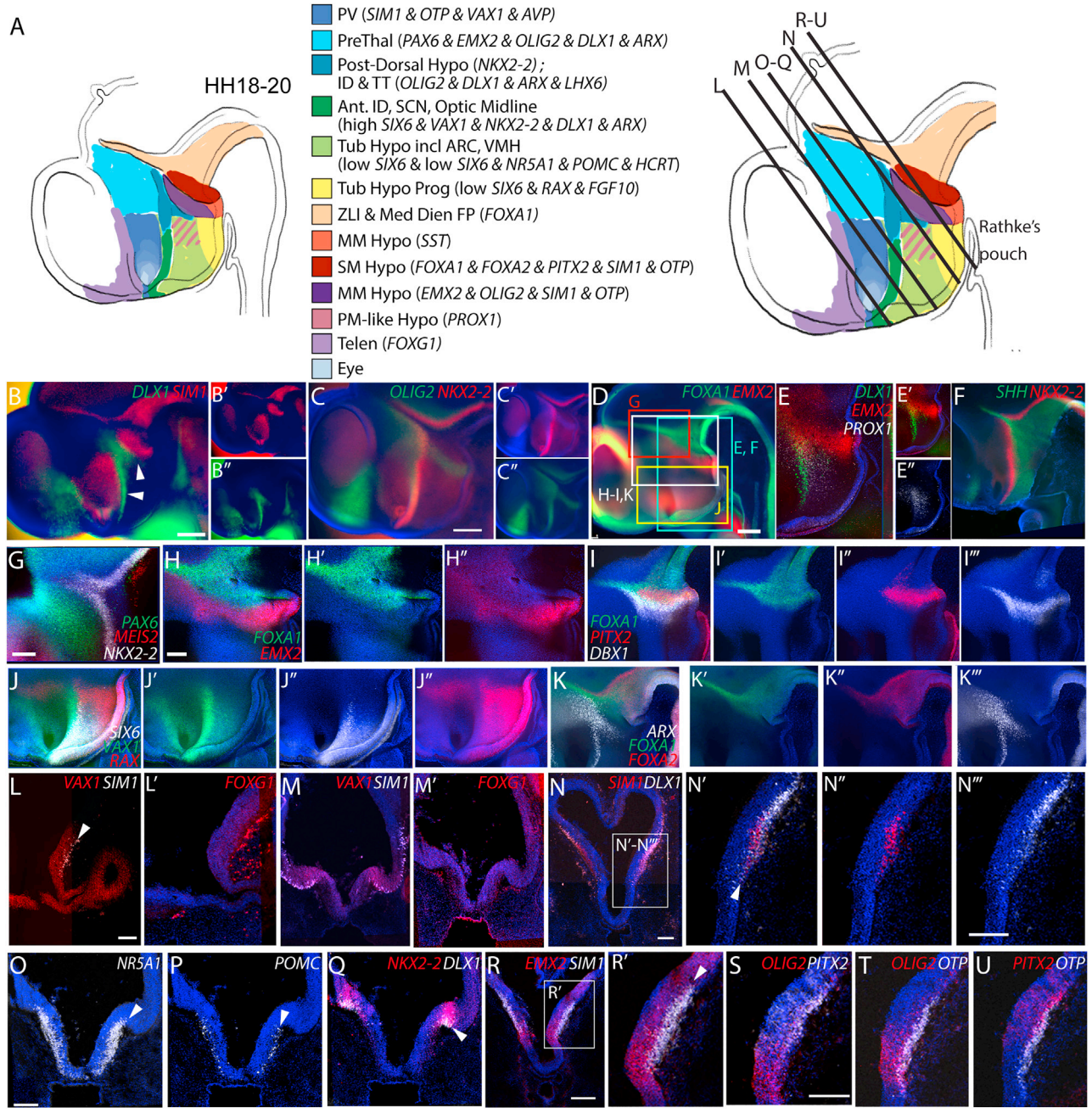

Figure 4. Hypothalamic regionalization at HH18–HH20

(A) Left: schematic sideview showing major hypothalamic progenitor regions at HH18–HH20 and their position within the forebrain and relative to Rathke's pouch; colored regions approximate their counterparts in Figures 2 and 3. Right: schematic showing planes of sections shown in (L)–(U).

(B–K) Maximum intensity projections of hemi-dissected HH18–HH20 heads after wholemount *in situ* HCR for combinations of regional progenitor markers. Anterior to the left. Arrowheads in (B) point to ID and TT. Boxes in (D) show regions shown in (E)–(K).

(L–U) Transverse sections of HH20 embryos after *in situ* HCR for combinations of regional and neuronal precursor markers. Boxes in (N) and (R) show regions shown in (N′)–(N‴) and (R′). Sections shown in (S)–(U) are serial adjacent to that in (R). Arrowheads in (L), (N′), (O)–(Q) and (R′) point to the mantle zone.

Scale bars, 100 μm (G, H, L, N, N‴, O, R, and S) and 250 μm (B–D). Markers shown in (N)–(N‴) and (Q)–(U) have been digitally overlaid after stripping and re-probing of single sections. PV, paraventricular; PM, premammillary; SCN, suprachiasmatic nucleus; ZLI, zona limitans intrathalamica. Other abbreviations as per Figures 1, 2, and 3.

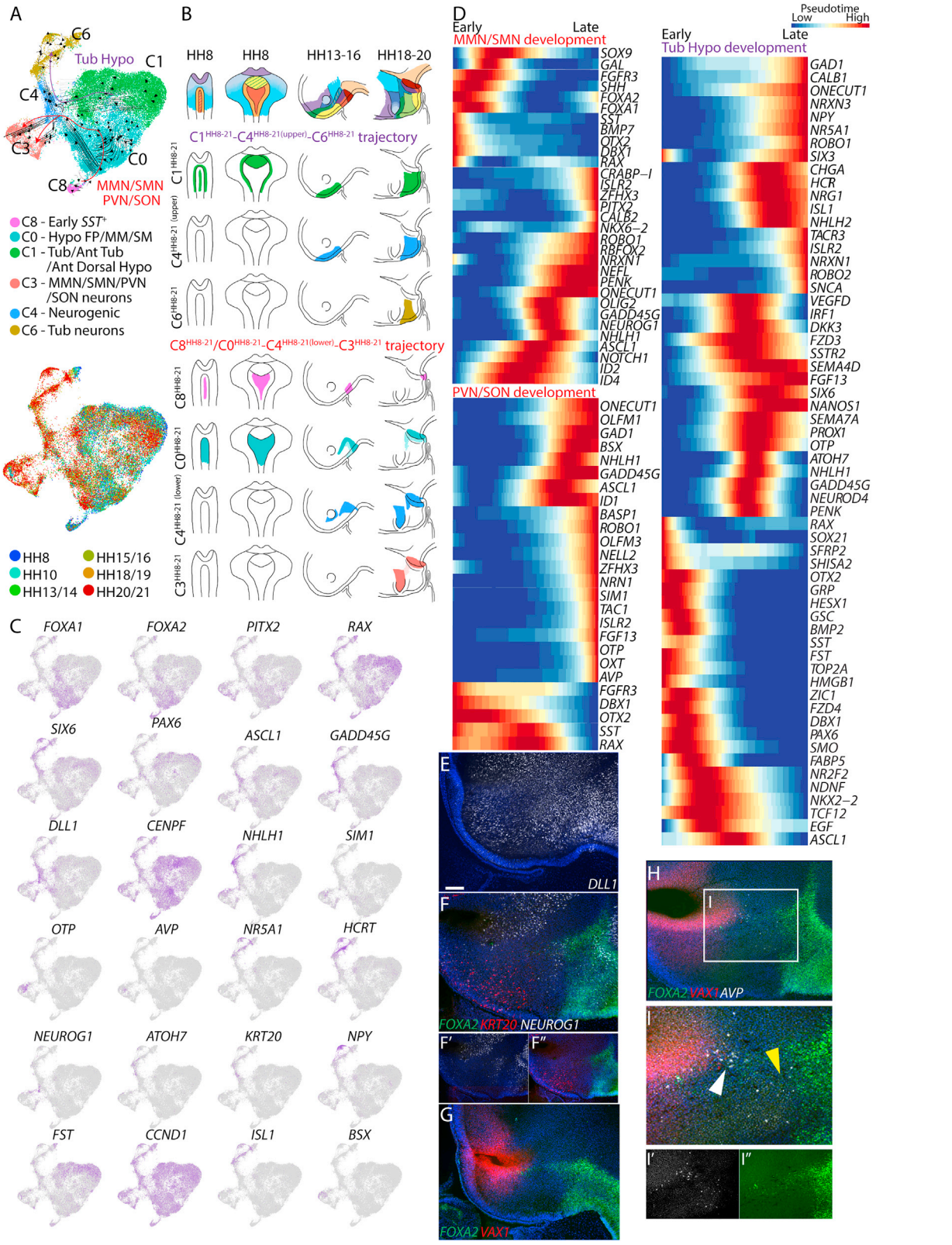

(legend on next page)

cell clusters ($C0^{HH8-21}$ and $C1^{HH8-21}$) converge into a cell cluster ($C4^{HH8-21}$) distinguished by *ASCL1/GADD45G/DLL1* but which still expresses cell-cycle markers (*CENPF/CCND1*) (Figures 5A–5C; Table S6). Similar populations have been observed in developing retina, cortex, and cerebellum and appear to correspond to progenitors undergoing terminal neurogenic divisions (Carter et al., 2018; Clark et al., 2019; Loo et al., 2019).

Two neuronal differentiation trajectories arise from the $C4^{HH8-21}$ neurogenic cluster. Cluster $C3^{HH8-21}$ corresponds to mammillary/paraventricular neuronal precursors (*PITX2/SIM1/OTP/AVP)* and cluster $C6^{HH8-21}$ corresponds to tuberal neuronal precursors (*NR5A1/ISL1/HCRT*) (Figures 5A–5C). $C1^{HH8-21}$–$C6^{HH8-21}$ and $C0^{HH8-21}$–$C3^{HH8-21}$ trajectories pass through upper and lower subdivisions of $C4^{HH8-21}$, respectively. This supports the idea that while neurogenic tuberal and mammillary/paraventricular progenitors express some common genes, these structures arise through two distinct differentiation programs.

Pseudotime analysis identified common and divergent patterns for dynamic gene expression in the distinct neurogenic trajectories. In each, *RAX/DBX1/SST/OTX2* expression is downregulated (Figure 5D). The tuberal trajectory downregulates prethalamic-like markers such as *PAX6/ZIC1/FST/BMP2/GSC* early on (Figure 5D). The mammillary trajectory initially expresses, then downregulates, floor-plate-like markers such as *FOXA1/FOXA2/SHH/BMP7* (Figure 5D). Neurogenic progenitors in both trajectories transiently express *ASCL1/NHLH1/GADD45G*; however, *NEUROG1* is also expressed in the paraventricular/mammillary trajectory and *ATOH7* and *KRT20* are expressed in the tuberal (Figure 5C). *ATOH7* plays an essential role in retinal ganglion cell survival but has not been previously linked to hypothalamic development (Brodie-Kommit et al., 2021). HCR validates these expression patterns. Thus, while *DLL1*-positive cells (i.e. $C4^{HH8-21}$ cells, both upper and lower) are detected in tuberal, posterior/mammillary, and paraventricular regions (Figure 5E), *NEUROG1* ($C4^{HH8-21}$ lower and $C3^{HH8-21}$) is restricted to mamillary and paraventricular domains, and *KRT20* ($C4^{HH8-21}$ upper and $C6^{HH8-21}$) is restricted to the tuberal domain (Figure 5F).

Many well-established regional and cell-type-specific markers are only detected in relatively mature cells at the tips of the trajectories. These include *NR5A1/HCRT/NPY* in the tuberal stream and *PITX2/SIM1/OTP/AVP* in the mammillary/paraventricular stream (Figure 5C). Both the tuberal and mammillary/paraventricular streams bifurcate by HH18 (Figure 5A). In the former, the two streams are distinguished by high versus absent expression of *NPY* (Figure 5C). In the latter, floor-plate-like/mammillary markers such as *PITX2/FOXA2* are distributed across both branches at HH20/21, but PVN-specific transcripts such as *OTP/AVP/BSX* are restricted to one branch (Figure 5C). One interpretation of this is that PVN-specific characteristics develop from a program common to mammillary and PVN-like neurons and that PVN neurons may arise from mammillary progenitors. In support of this, HCR analysis of HH17 embryos shows a strip of *FOXA2*-positive cells, along the ID, extending to the *VAX1*-positive paraventricular domain (Figure 5G; see also Figures 3F and 3J; HH14–HH15). At HH19, *AVP*-positive cells overlap this *FOXA2*-positive domain at the edge of the paraventricular region (Figures 5H and 5I). Scattered *AVP*-positive cells are also seen in the dorsal mammillary region partially overlapping with *FOXA2* (Figures 5H and 5I). Although we cannot exclude the possibility that *AVP*-positive paraventricular neurons arise directly from *VAX1*-positive progenitors, this suggests that some or all *AVP*-positive neurons may arise from floor-plate-like progenitors that undergo tangential migration from the mammillary to the paraventricular region.

In summary, these data describe chick hypothalamic development in detail, linking early stages of induction (that were partially described in previous work) through patterning and the beginning of neurogenesis, up to a point in development where the equivalent stages in mouse are more tractable to study and have been more extensively explored (Figure 1A).

Evolutionary conservation of hypothalamic neuronal precursor identity

We next set out to identify molecular similarities between neuronal precursor subtypes identified in the developing chick, mouse, and human. To do this, we performed UMAP analysis of the aggregated HH18/19 and HH20/21 scRNA-seq datasets, computationally extracted all postmitotic neural precursors, and separately clustered these to identify cell-type-specific markers (Figure 6A; Table S7). We identified eight clusters: three tuberal, three mammillary, one paraventricular, and one prethalamic/ID/TT-like. Tuberal clusters ($C0^{HH18-21}$, $C1^{HH18-21}$, and $C3^{HH18-21}$) all express *SIX3/SIX6/ISL1* but can be distinguished: C0 expresses the lowest levels of *NR5A1*, high *POMC*, no *NPY*, and low *HCRT*; $C1^{HH18-21}$ expresses high *NHLH1/NPY/HCRT* and no *POMC*; and $C3^{HH18-21}$ expresses high *POMC/HCRT* and low *NPY* (Figure 6B; Table S7). This implies that distinct populations of *POMC*- and *NPY*-expressing neurons are already emerging at this stage, well in advance of mice (Padilla et al., 2010).

Mammillary ($C2^{HH18-21}$, $C5^{HH18-21}$, and $C7^{HH18-21}$) and PVN/SON ($C4^{HH18-21}$) clusters can likewise be distinguished. $C4^{HH18-21}$ cells selectively express *SIM1/OTP/OXT/AVP* (Figure 6B; Table S7) but also express high levels of *OLIG2* and *NEFL* and, unlike clusters 2 and 5, do not express *FOXA1/2/NKX6-2/PITX2* (Figure 6B; Table S7). $C2^{HH18-21}$, based on

Figure 5. Gene networks controlling hypothalamic regionalization

(A) UMAP plot of clusters across the entire period of hypothalamic development showing developmental trajectories obtained from RNA velocity analysis of the tuberal, PVN/SON, and mammillary hypothalamus (top), and UMAP plot showing developmental timepoints across hypothalamic development (bottom).

(B) Schematic showing approximate spatial locations of cells in the HH8–HH21 clusters.

(C) UMAP plots for selected genes across hypothalamic development.

(D) Pseudotime showing gene expression changes through mammillary/supramammillary, PVN/SON, and tuberal hypothalamic development.

(E–I) Maximum intensity projections of hemi-dissected HH17–HH20 heads after wholemount HCR single, double, or triple *in situ* hybridization with combinations of regional progenitor and neurogenic markers. Anterior is oriented to the left. Box in (H) shows region shown in (I)–(I″).

Scale bars:100 μm. SON, supraoptic nucleus. Other abbreviations as per Figures 1, 2, 3, and 4.

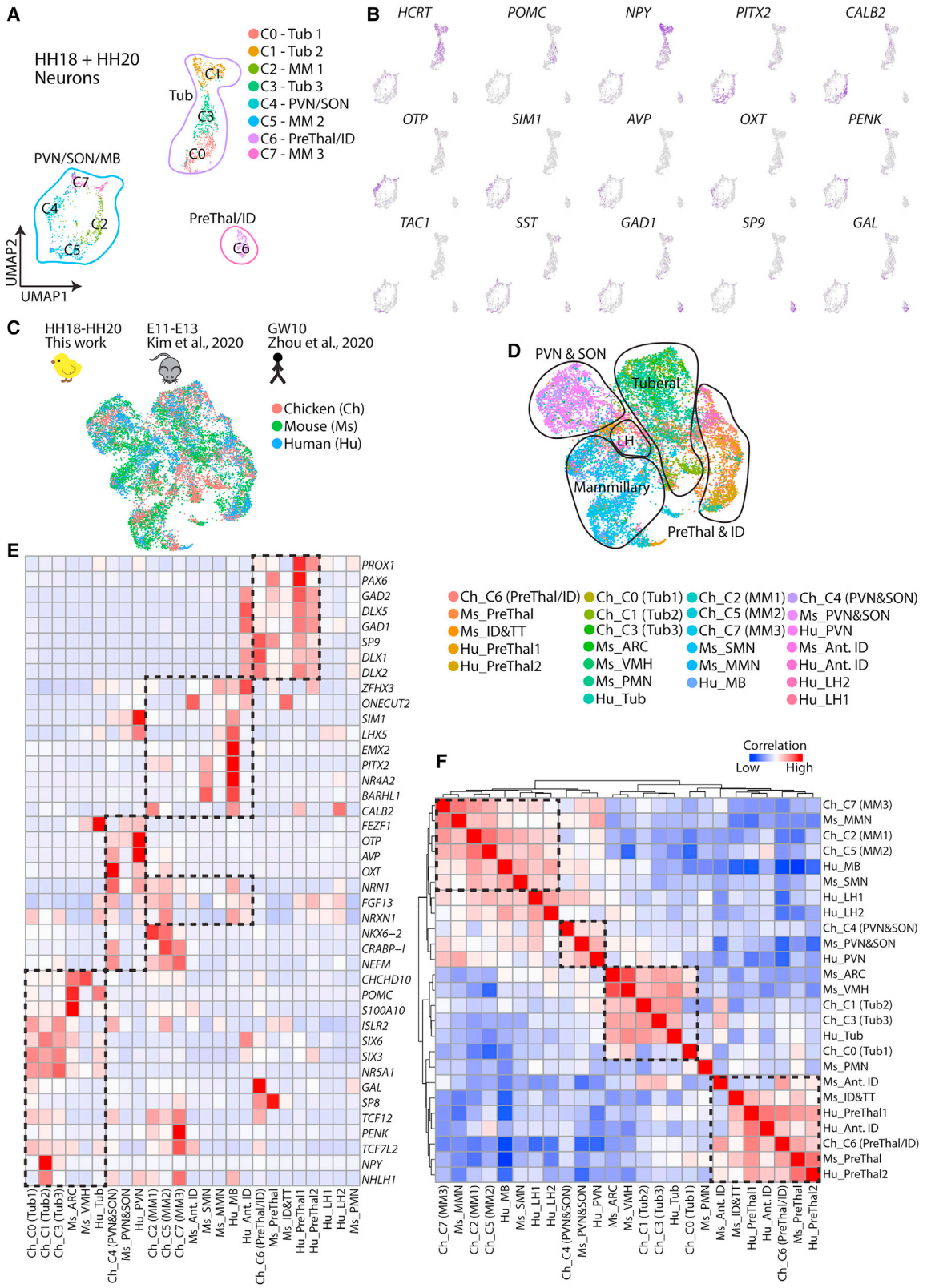

(legend on next page)

enriched expression of *SIM1/CALB2* (Figure 6B), may correspond to neurons of the mammillary nucleus. $C5^{HH18-21}$ cells express high levels of *TAC1* (Figure 6B; Table S7) and likely correspond to immature supramammillary neurons. $C7^{HH18-21}$ cells express *SST/DBX1* and so likely correspond to immature ventral mammillary neurons (Figure 6B; Table S7). Major subdivisions of the posterior hypothalamus can thus be distinguished at this stage.

Cluster $C6^{HH18-21}$ selectively expresses canonical markers of hypothalamic GABAergic neural precursors, such as *DLX1/2* and *GAD1/2* (Figures 6B, 6E, and 6F; Table S7), along with the transcription factors *SP8/SP9* (Table S7). These genes are expressed in the prethalamus, ID, and TT in mouse (Kim et al., 2020; Shimogori et al., 2010) and in the chick ID at HH20/21 (Figure 4B). Since this cluster shows little expression of the prethalamic marker *GSX2* (Kim et al., 2020; Shimogori et al., 2010), neurons in $C6^{HH18-21}$ represent hypothalamic ID and TT neurons. $C6^{HH18-21}$ showed much higher *GAL* expression, higher *DLX1/2* expression, and lower *DLX5* and *GAD2* expression relative to mouse and human. Since *DLX1/2* directly regulates *DLX5* expression and precedes the expression of GABAergic markers, this may imply that cells in chick $C6^{HH18-21}$ are less mature than their mammalian counterparts rather than reflecting species-specific differences in gene expression.

We next directly compared these chick neuronal precursor clusters to clusters previously annotated in scRNA-seq studies in E11–E13 mouse hypothalamus (Kim et al., 2020) and gestational week 10 human hypothalamus (Zhou et al., 2020). Tuberal clusters ($C0^{HH18-21}$, $C1^{HH18-21}$, and $C3^{HH18-21}$) closely matched mouse arcuate and ventromedial hypothalamic clusters and the human tuberal hypothalamic cluster (Figures 6C–6F). A few notable species-specific differences were observed. *NPY* and *NHLH1* expressions were highly enriched in chick $C1^{HH18-21}$ but not in humans or mice. Mouse arcuate and human tuberal clusters also showed substantially higher levels of *POMC* than did chick, while mouse arcuate and ventromedial clusters showed higher expression of *CHCHD10* than did chick or human (Figure 6E).

$C4^{HH18-21}$ chick cells most closely resemble the PVN/supraoptic nucleus (SON) mouse and human PVN clusters (Figure 6E). Chick $C4^{HH18-21}$ cells more closely resemble human PVN than the mouse PVN/SON, with both selectively expressing *FGF13/NRN1/OXT/AVP* (Figure 6E). $C4^{HH18-21}$ cells express several genes not enriched in humans or mice—including *TCF12/NEFM/CRABP1* (Figure 6E)—but do not express the transcription factor *LHX5*, which is expressed in both mouse and human.

Mammillary clusters $C2^{HH18-21}$ and $C5^{HH18-21}$ resemble the human mammillary cluster. While both $C2^{HH18-21}$ and $C5^{HH18-21}$ express *PITX2*, neither closely resembles the mouse supramammillary cluster (Figures 6E and 6F). The human mammillary cluster, however, expresses supramammillary markers such as *NR4A2/BARHL1*, suggesting that this represents both mammillary and supramammillary regions (Kim et al., 2020). No clear counterpart for $C7^{HH18-21}$ is detected. No clear counterparts to the premammillary cluster in mice or the lateral hypothalamic clusters in humans are detected in chick, consistent with our finding that these structures are not clearly defined at this age.

Inhibition of hypothalamic induction by prethalamic-derived follistatin

Our scRNA-seq and HCR analyses provide a wealth of candidate genes for experimental investigations of hypothalamic development. Our analyses suggest that *PAX6*-expressing prethalamic-like cells undergo conversion to hypothalamic progenitors. We explored this idea by building on two previous studies. The first delineated the spatial position of the future hypothalamus from HH4–HH8 (Dale et al., 1997). The second defined the onset of hypothalamic specification measured by *NKX2-1* expression, showing that it had not yet begun at HH4 but was initiated by HH6 (Ohyama et al., 2005). Using an *ex vivo* assay, we observed a direct conversion of prethalamic-like to hypothalamic identity. In cultured HH4 explants, most cells expressed PAX6, but no NKX2-1 was detected, while in HH6 explants, NKX2-1-positive cells were detected, many of which co-expressed PAX6 (Figures 7A–7C, arrows). This confirms that hypothalamic progenitors are induced from prethalamic-like progenitors.

Nodal from prechordal mesoderm triggers hypothalamic induction and patterning (Mathieu et al., 2002; Müller et al., 2000; Patten et al., 2003), and scRNA-seq analysis reveals that *PAX6*-expressing prethalamic-like cells express *FST* at HH8–HH10 (Figures 2H and 2T). Since FST is a potent Nodal antagonist, prethalamic-derived FST may limit the lateral extent of hypothalamic induction. To test this hypothesis, an FST neutralizing antibody (anti-FST) or recombinant FST was injected onto the hypothalamus of HH5/6 embryos *in vivo*, which were then developed to HH14 (Figures 7C–7F). Anti-FST increased the *NKX2-1/SHH*-positive hypothalamic domain relative to controls and reduced the prethalamic *PAX6* domain, although *PAX6* expression in Rathke's pouch was unaltered (Figures 7D and 7E). Conversely, no *SHH/NKX-2.1*-positive cells were seen in embryos treated with recombinant FST (Figure 7F). *SHH* expression was seen along the ventral midline, which was expanded relative to controls (Figure 7F).

In parallel, we performed *ex vivo* studies, dissecting out prospective hypothalamus at HH4 and culturing explants in control media or with anti-FST until the equivalent of HH14 (Figures 7G and 7H). Control explants showed separate domains of *PAX6* and *SHH* expression, with almost no detectable *NKX-2.1* expression (Figure 7G). In contrast, explants exposed to anti-FST downregulated *PAX6* and upregulated *NKX-2.1* throughout

Figure 6. Evolutionary conservation of hypothalamic neuronal precursor identity

(A–D) UMAP plots showing (A) distribution of mature hypothalamic and prethalamic/ID neurons at HH18/20, (B) expression of genes enriched in different hypothalamic neuronal clusters, (C) integrated dataset, and (D) integrated clusters of developing chicken hypothalamus (HH18/19–HH20/21), mouse hypothalamus (E11–E13 [Kim et al., 2020]), and human hypothalamus (GW10 [Zhou et al., 2020]).

(E) Heatmap showing conserved key gene expression patterns between neuronal precursor clusters in chicken, mouse, and human developing hypothalami.

(F) Correlation heatmap for developing chicken hypothalamus (HH18/19–HH20/21), mouse hypothalamus (E11–E13 [Kim et al., 2020]), and human hypothalamus (GW10 [Zhou et al., 2020]).

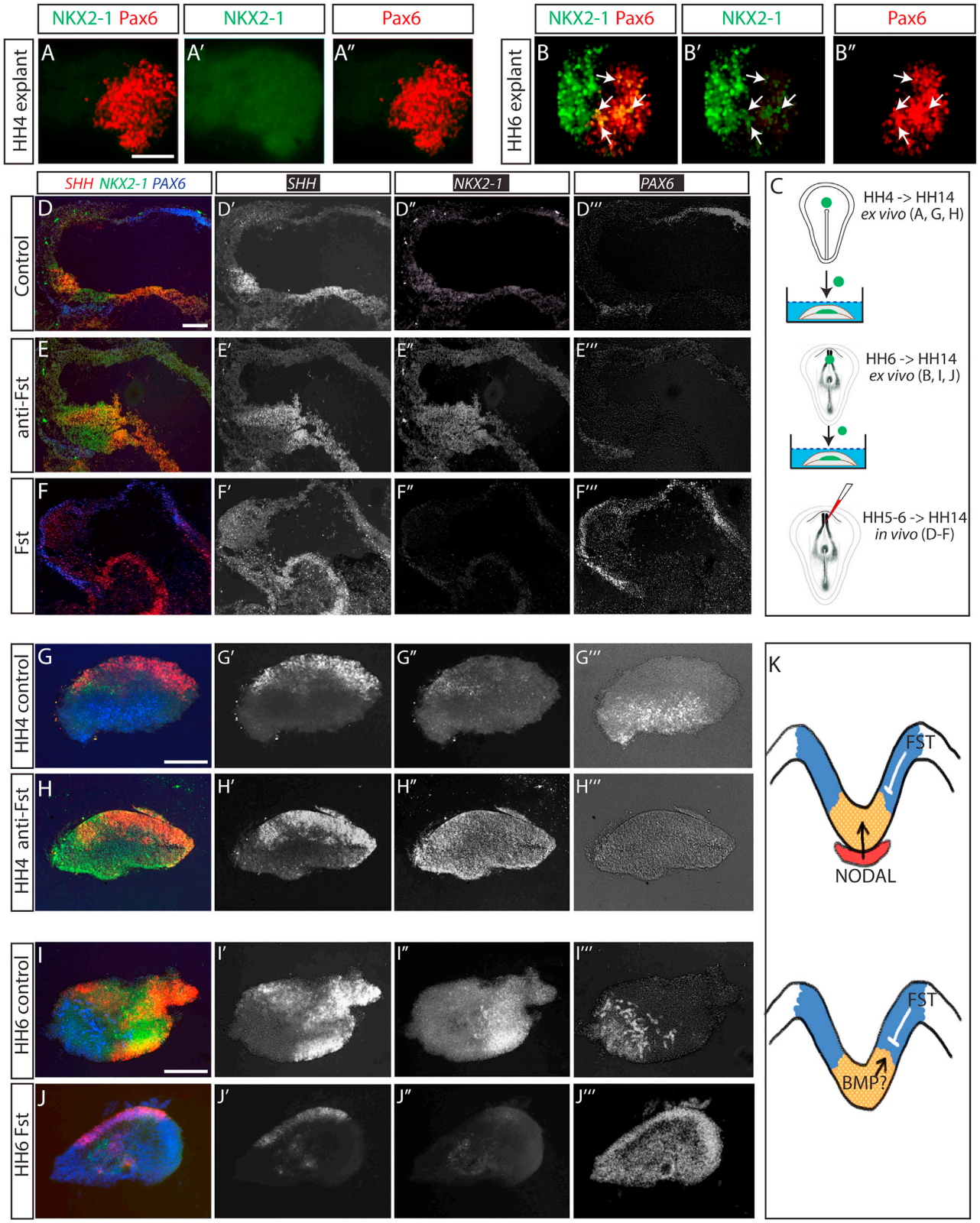

(legend on next page)

the explant, with many *SHH*/*NKX-2.1*-positive cells detected (Figure 7H).

Finally, we dissected the prospective hypothalamus at HH6, at the onset of its specification. Explants were cultured in control media or with recombinant FST until the HH14 equivalent. Robust hypothalamic differentiation was detected in controls, with many *NKX-2.1*/*SHH*-positive cells seen and a separate domain of *PAX6*-positive cells (Figure 7I). In contrast, exposure to FST almost eliminated *NKX-2.1* expression, and *PAX6*-positive cells dominated the explant (Figure 7I). We conclude that prethalamic-derived FST inhibits hypothalamic specification and constrains the size of the developing hypothalamus.

DISCUSSION

This study provides a comprehensive roadmap for the molecular mechanisms controlling hypothalamic induction, regionalization, and initiation of neurogenesis, made possible by using the chick model system, where the hypothalamus is larger and more slowly developing than the mouse. It is unsurprising, given the central role of the hypothalamus in regulating many evolutionarily ancient innate behaviors, that the spatial organization of the chick hypothalamus is similar to that of the mammalian hypothalamus during early neurogenesis. This study provides unprecedented insight into evolutionarily conserved processes that orchestrate hypothalamic patterning and regionalization.

New molecular markers that we identify here show that the HH8 hypothalamus closely resembles a floor-plate-like domain sitting directly adjacent to prethalamus-like tissue. The prethalamus is the earliest-developing forebrain structure (Staudt and Houart, 2007), and *OLIG2*-expressing cells are seen in the prospective prethalamus as early as HH8. Transiently (at HH8) *OLIG2*-positive cells concentrically surround the developing hypothalamic floor plate—including *SIX6* expressing cells—likely prefiguring the position of the ID. Our study provides clear evidence to support the idea that the hypothalamus arises from prethalamus-like cells. This contradicts the predictions of the prosomere model, which places the prethalamus posterior to the hypothalamus in prosomere 3 and the telencephalon dorsal to the hypothalamus, as part of the secondary prosencephalon (Puelles, 2019). Further studies will help clarify the broader organization of the developing vertebrate forebrain.

Furthermore, our study demonstrates that prethalamus-derived FST constrains the size of the developing hypothalamus. Genetic analysis has shown that *NKX2-1* promotes hypothalamic identity while simultaneously repressing prethalamic identity (Kim et al., 2020) and that FST may inhibit a factor that induces *NKX2-1*. While Nodal is a top candidate for this factor, our explant cultures include no prechordal mesoderm, and no Nodal is detected in hypothalamic cells by scRNA-seq, suggesting that another FST target may mediate these effects. One candidate is *BMP2*, which is expressed in a complementary pattern to *FST* at HH8 and HH10 (Figure 7F'). BMP2 interacts with SHH to induce and pattern the hypothalamus (Dale et al., 1997; Manning et al., 2006; Ohyama et al., 2005), while in the posterior neural tube, FST modulates BMP signaling to regulate dorsoventral neural tube patterning with SHH (Liem et al., 2000). Interactions between BMPs, SHH, and FST are likely to underlie hypothalamic induction. Further studies will be required to dissect the relative contribution of these factors and the precise mechanism of action of FST.

Our study markedly extends previous characterizations of floor-plate-like hypothalamic progenitors and demonstrates their expansion between HH8 and HH10 (Dale et al., 1997, 1999). Further, both scRNA-seq and HCR identify two spatially and molecularly distinct clusters of hypothalamic progenitors in the HH10 embryo. The first initially expresses floor-plate-like markers, such as *FOXA2*, but later generates neurons of the posterior (mammillary/supramammillary) nuclei and possibly also the PVN. The second—which expresses *SIX6*/*RAX*/*FGF10*—generates neurons of the tuberal hypothalamus, including the ventromedial and arcuate nuclei.

The finding that the mammillary/supramammillary and paraventricular hypothalamus share a similar developmental program is surprising, as they are located at opposite ends of the hypothalamus. At HH20, mammillary/supramammillary and paraventricular hypothalamic neural precursors cluster together, while HCR analysis shows that the paraventricular marker *AVP* is also found in mammillary regions (Figures 5H and 5I), in agreement with previous studies (Caqueret et al., 2005). Moreover, progenitors at the anterior and posterior borders of the mouse hypothalamus co-express several genes, including *LHX5*/*SIM1*/*NEUROG2* (Kim et al., 2020; Shimogori et al., 2010). While similar neuronal differentiation programs may mask underlying differences in progenitor origin (Mayer et al., 2018), an intriguing possibility is that *AVP*-expressing neurons in the anterodorsal hypothalamus have migrated into this position from the mammillary region rather than being born locally from *VAX1*/*RAX*-positive progenitors. Differential Wnt signaling, which posteriorizes the zebrafish and mouse hypothalamus, may distinguish the posterior (mammillary/supramammillary) and paraventricular divisions of the hypothalamus (Lee et al., 2006; Newman et al., 2018).

Figure 7. Inhibition of hypothalamic induction by prethalamic-like derived follistatin

(A and B) Immunohistochemical analysis of PAX6 and NKX2-1 in HH4 cultured explant (A–A″) or HH6 cultured explant (B–B″) (n = 5 explants/condition).

(C) Schematic depicts *ex vivo* explant experiments and *in vivo* gain- or loss-of-function experiments.

(D–F) *In situ* HCR showing *SHH*, *NKX2-1*, and *PAX6* in sagittal sections of HH14 embryos after *in vivo* injection (C, bottom schematic) of PBS (D), anti-FST (E), or FST (F) at HH5–HH6. n = 3 embryos/condition.

(G and H) *In situ* HCR showing *SHH*, *NKX2-1*, and *PAX6* in sections of explants cultured from HH4–HH14 (C, top schematic) in either control medium (G) or anti-FST (H).

(I and J) HCR showing *SHH*, *NKX2-1*, and *PAX6* in sections of explants cultured from HH6–HH14 (C, middle schematic) in either control medium (I) or anti-Fst (J). n = 7–10 explants/condition.

(K) Schematic showing FST regulation of hypothalamus development.

Scale bars, 100 μm.

By HH18, the structure of the chick hypothalamus resembles that of the E11.5 mouse, and counterparts of most major chick neuronal precursor populations are observed in E11–E13 mice and gestational week 10 (GW10) humans. Paraventricular and mammillary progenitor populations can be distinguished, and prethalamic markers extend into the basal hypothalamus, anteriorly via the ID and ventrally via the TT. In the tuberal hypothalamus, markers of both the ventromedial hypothalamus and arcuate nuclei, such as *NR5A1* and *POMC*, are observed, although neither structure is yet spatially distinct.

Previous studies have highlighted the importance of a detailed understanding of hypothalamic development to human health. Congenital metabolic disorders and obesity can result from mutations in transcription factors that control hypothalamic patterning (Blanchet et al., 2017; Holder et al., 2000). Mutations in genes identified in this study may contribute to multigenic disorders that may have a hypothalamic origin, such as type 2 diabetes, sleep disorders, and depression (Bao et al., 2008; Biran et al., 2015; Dearden and Ozanne, 2015). Understanding mechanisms that control early hypothalamic development will also guide efforts aimed at inducing differentiation of specific hypothalamic neuronal subtypes from embryonic stem cells (ESCs) or induced pluripotent stem cells (iPSCs) (Merkle et al., 2015; Nagasaki et al., 2015; Seifinejad et al., 2019; Wang et al., 2016) and for the directed reprogramming of hypothalamic glial cells (Kano et al., 2019; Yoo et al., 2021). Ultimately, cell-based approaches such as these may allow for directed rewiring of hypothalamic circuitry, enabling treatment of a broad range of homeostatic disorders.

Limitations of the study

Due to the difficulty in obtaining large amounts of tissue at HH6 and inaccurately dissecting the hypothalamus during head turning, our analyses do not profile gene expressions prior to HH8 or at HH11/12. Since hypothalamic floor-plate-like specification is initiated at HH6, and neurogenesis is initiated around HH12, our study may not capture all gene expression changes that regulate these processes. The inclusion of samples older than HH21 would also facilitate accurate cross-species comparison of evolutionarily conserved and species-specific patterns of gene expression.

STAR★METHODS

Detailed methods are provided in the online version of this paper and include the following:

SUPPLEMENTAL INFORMATION

Supplemental information can be found online at https://doi.org/10.1016/j.celrep.2021.110251.

ACKNOWLEDGMENTS

We thank A. Fletcher, A. Furley, M. Towers, I. Barbaric, J. Kebschull, B. James, W. Yap, L. Duncan, J. Ling, and T. Shimogori for helpful comments on the manuscript. We thank Transcriptomics and Deep Sequencing Core (Johns Hopkins) for sequencing of scRNA-seq libraries. This work was supported by the Wellcome Trust (212247/Z/18/Z) to M.P., NIH (R01DK108230) to S. Blackshaw., and the Maryland Stem Cell Research Fund (2019-MSCRFF-5124) to D.W.K.

AUTHOR CONTRIBUTIONS

S. Blackshaw and M.P. conceived and supervised the study. D.W.K. generated all scRNA-seq data. D.W.K., C.S., and W.D. analyzed scRNA-seq data. K.C., S. Burbridge, and M.P. dissected chick hypothalamuses. E.P., K.C, S. Burbridge., E.M., and I.G. conducted HCR analysis and imaging. E.M., K.O., and M.P. performed explant and *in vivo* work. E.P. developed schematics. D.W.K., E.P., K.C., M.P., and S. Blackshaw drafted the manuscript. All authors edited the manuscript.

DECLARATION OF INTERESTS

The authors declare no competing interests.

Received: April 23, 2021
Revised: September 13, 2021
Accepted: December 20, 2021
Published: January 18, 2022

REFERENCES

Alles, J., Karaiskos, N., Praktiknjo, S.D., Grosswendt, S., Wahle, P., Ruffault, P.-L., Ayoub, S., Schreyer, L., Boltengagen, A., Birchmeier, C., et al. (2017). Cell fixation and preservation for droplet-based single-cell transcriptomics. BMC Biol. *15*, 44.

Antin, P.B., Yatskievych, T.A., Davey, S., and Darnell, D.K. (2014). GEISHA: an evolving gene expression resource for the chicken embryo. Nucleic Acids Res. *42*, D933–D937.

Aslanpour, S., Han, S., Schuurmans, C., and Kurrasch, D.M. (2020). Neurog2 acts as a classical proneural gene in the ventromedial hypothalamus and is required for the early phase of neurogenesis. J. Neurosci. *40*, 3549–3563.

Bailey, A.P., Bhattacharyya, S., Bronner-Fraser, M., and Streit, A. (2006). Lens specification is the ground state of all sensory placodes, from which FGF promotes olfactory identity. Dev. Cell *11*, 505–517.

Bao, A.-M., Meynen, G., and Swaab, D.F. (2008). The stress system in depression and neurodegeneration: focus on the human hypothalamus. Brain Res. Rev. *57*, 531–553.

Bedont, J.L., LeGates, T.A., Slat, E.A., Byerly, M.S., Wang, H., Hu, J., Rupp, A.C., Qian, J., Wong, G.W., Herzog, E.D., et al. (2014). Lhx1 controls terminal differentiation and circadian function of the suprachiasmatic nucleus. Cell Rep *7*, 609–622.

Bedont, J.L., Newman, E.A., and Blackshaw, S. (2015). Patterning, specification, and differentiation in the developing hypothalamus. Wiley Interdiscip. Rev. Dev. Biol. *4*, 445–468.

Bergen, V., Lange, M., Peidli, S., Wolf, F.A., and Theis, F.J. (2020). Generalizing RNA velocity to transient cell states through dynamical modeling. Nat. Biotechnol. *38*, 1408–1414.

Biran, J., Tahor, M., Wircer, E., and Levkowitz, G. (2015). Role of developmental factors in hypothalamic function. Front. Neuroanat. *9*, 47.

Blackshaw, S., Scholpp, S., Placzek, M., Ingraham, H., Simerly, R., and Shimogori, T. (2010). Molecular pathways controlling development of thalamus and hypothalamus: from neural specification to circuit formation. J. Neurosci. *30*, 14925–14930.

Blanchet, P., Bebin, M., Bruet, S., Cooper, G.M., Thompson, M.L., Duban-Bedu, B., Gerard, B., Piton, A., Suckno, S., Deshpande, C., et al. (2017). MYT1L mutations cause intellectual disability and variable obesity by dysregulating gene expression and development of the neuroendocrine hypothalamus. PLoS Genet *13*, e1006957.

Brodie-Kommit, J., Clark, B.S., Shi, Q., Shiau, F., Kim, D.W., Langel, J., Sheely, C., Schmidt, T., Badea, T., Glaser, T., et al. (2021). Atoh7-independent specification of retinal ganglion cell identity. Sci. Adv *7*, eabe4983.

Browaeys, R., Saelens, W., and Saeys, Y. (2020). NicheNet: modeling intercellular communication by linking ligands to target genes. Nat. Methods. *17*, 159–162.

Burbridge, S., Stewart, I., and Placzek, M. (2016). Development of the neuroendocrine hypothalamus. Compr. Physiol. *6*, 623–643.

Butler, A., Hoffman, P., Smibert, P., Papalexi, E., and Satija, R. (2018). Integrating single-cell transcriptomic data across different conditions, technologies, and species. Nat. Biotechnol. *36*, 411–420.

Caqueret, A., Coumailleau, P., and Michaud, J.L. (2005). Regionalization of the anterior hypothalamus in the chick embryo. Dev. Dyn. *233*, 652–658.

Carter, R.A., Bihannic, L., Rosencrance, C., Hadley, J.L., Tong, Y., Phoenix, T.N., Natarajan, S., Easton, J., Northcott, P.A., and Gawad, C. (2018). A single-cell transcriptional atlas of the developing murine cerebellum. Curr. Biol. *28*, 2910–2920.e2.

Chen, X., Wyler, S.C., Li, L., Arnold, A.G., Wan, R., Jia, L., Landy, M.A., Lai, H.C., Xu, P., and Liu, C. (2020). Comparative transcriptomic analyses of developing melanocortin neurons reveal new regulators for the anorexigenic neuron identity. J. Neurosci. *40*, 3165–3177.

Clark, B.S., Stein-O'Brien, G.L., Shiau, F., Cannon, G.H., Davis-Marcisak, E., Sherman, T., Santiago, C.P., Hoang, T.V., Rajaii, F., James-Esposito, R.E., et al. (2019). Single-cell RNA-seq analysis of retinal development identifies NFI factors as regulating mitotic exit and late-born cell specification. Neuron. *102*, 1111–1126.e5.

Costes, S.V., Daelemans, D., Cho, E.H., Dobbin, Z., Pavlakis, G., and Lockett, S. (2004). Automatic and quantitative measurement of protein-protein colocalization in live cells. Biophys. J. *86*, 3993–4003.

Dalal, J., Roh, J.H., Maloney, S.E., Akuffo, A., Shah, S., Yuan, H., Wamsley, B., Jones, W.B., de Guzman Strong, C., Gray, P.A., et al. (2013). Translational profiling of hypocretin neurons identifies candidate molecules for sleep regulation. Genes Dev. *27*, 565–578.

Dale, J.K., Vesque, C., Lints, T.J., Sampath, T.K., Furley, A., Dodd, J., and Placzek, M. (1997). Cooperation of BMP7 and SHH in the induction of forebrain ventral midline cells by prechordal mesoderm. Cell. *90*, 257–269.

Dale, K., Sattar, N., Heemskerk, J., Clarke, J.D., Placzek, M., and Dodd, J. (1999). Differential patterning of ventral midline cells by axial mesoderm is regulated by BMP7 and chordin. Development. *126*, 397–408.

Dearden, L., and Ozanne, S.E. (2015). Early life origins of metabolic disease: developmental programming of hypothalamic pathways controlling energy homeostasis. Front. Neuroendocrinol. *39*, 3–16.

Eachus, H., Bright, C., Cunliffe, V.T., Placzek, M., Wood, J.D., and Watt, P.J. (2017). Disrupted-in-Schizophrenia-1 is essential for normal hypothalamic-pituitary-interrenal (HPI) axis function. Hum. Mol. Genet. *26*, 1992–2005.

Ferran, J.L., Sánchez-Arrones, L., Bardet, S.M., Sandoval, J.E., Martínez-de-la-Torre, M., and Puelles, L. (2008). Early pretectal gene expression pattern shows a conserved anteroposterior tripartition in mouse and chicken. Brain Res. Bull. *75*, 295–298.

Fu, T., Towers, M., and Placzek, M.A. (2017). Progenitors give rise to the chick hypothalamus by rostral and caudal growth and differentiation. Development. *144*, 3278–3288.

Garcia-Lopez, R., Pombero, A., and Martinez, S. (2009). Fate map of the chick embryo neural tube. Dev. Growth Differ. *51*, 145–165.

Hamburger, V., and Hamilton, H.L. (1992). A series of normal stages in the development of the chick embryo. 1951. Dev. Dyn. *195*, 231–272.

Holder, J.L., Jr., Butte, N.F., and Zinn, A.R. (2000). Profound obesity associated with a balanced translocation that disrupts the SIM1 gene. Hum. Mol. Genet. *9*, 101–108.

Ibrahim, M.M., and Kramann, R. (2019). genesorteR: feature ranking in clustered single cell data. bioRxiv. https://doi.org/10.1101/676379.

Kano, M., Suga, H., Ishihara, T., Sakakibara, M., Soen, M., Yamada, T., Ozaki, H., Mitsumoto, K., Kasai, T., Sugiyama, M., et al. (2019). Tanycyte-like cells derived from mouse embryonic stem culture show hypothalamic neural stem/progenitor cell functions. Endocrinology *160*, 1701–1718.

Kim, D.W., Washington, P.W., Wang, Z.Q., Lin, S.H., Sun, C., Ismail, B.T., Wang, H., Jiang, L., and Blackshaw, S. (2020). The cellular and molecular landscape of hypothalamic patterning and differentiation from embryonic to late postnatal development. Nat. Commun. *11*, 4360.

Kim, D.W., Liu, K., Wang, Z.Q., Zhang, Y.S., Bathini, A., Brown, M.P., Lin, S.H., Washington, P.W., Sun, C., Lindtner, S., et al. (2021). Gene regulatory networks controlling differentiation, survival, and diversification of hypothalamic Lhx6-expressing GABAergic neurons. Commun. Biol. *4*, 95.

Korsunsky, I., Millard, N., Fan, J., Slowikowski, K., Zhang, F., Wei, K., Baglaenko, Y., Brenner, M., Loh, P.-R., and Raychaudhuri, S. (2019). Fast, sensitive and accurate integration of single-cell data with Harmony. Nat. Methods. *16*, 1289–1296.

La Manno, G., Soldatov, R., Zeisel, A., Braun, E., Hochgerner, H., Petukhov, V., Lidschreiber, K., Kastriti, M.E., Lönnerberg, P., Furlan, A., et al. (2018). RNA velocity of single cells. Nature. *560*, 494–498.

Larsen, C.W., Zeltser, L.M., and Lumsden, A. (2001). Boundary formation and compartition in the avian diencephalon. J. Neurosci. *21*, 4699–4711.

Lee, B., Kim, J., An, T., Kim, S., Patel, E.M., Raber, J., Lee, S.-K., Lee, S., and Lee, J.W. (2018). Dlx1/2 and Otp coordinate the production of hypothalamic GHRH- and AgRP-neurons. Nat. Commun. *9*, 2026.

Lee, J.E., Wu, S.-F., Goering, L.M., and Dorsky, R.I. (2006). Canonical Wnt signaling through Lef1 is required for hypothalamic neurogenesis. Development. *133*, 4451–4461.

Liem, K.F., Jr., Jessell, T.M., and Briscoe, J. (2000). Regulation of the neural patterning activity of sonic hedgehog by secreted BMP inhibitors expressed by notochord and somites. Development. *127*, 4855–4866.

Liu, J., Merkle, F.T., Gandhi, A.V., Gagnon, J.A., Woods, I.G., Chiu, C.N., Shimogori, T., Schier, A.F., and Prober, D.A. (2015). Evolutionarily conserved regulation of hypocretin neuron specification by Lhx9. Development. *142*, 1113–1124.

Loo, L., Simon, J.M., Xing, L., McCoy, E.S., Niehaus, J.K., Guo, J., Anton, E.S., and Zylka, M.J. (2019). Single-cell transcriptomic analysis of mouse neocortical development. Nat. Commun. *10*, 134.

Lu, F., Kar, D., Gruenig, N., Zhang, Z.W., Cousins, N., Rodgers, H.M., Swindell, E.C., Jamrich, M., Schuurmans, C., Mathers, P.H., et al. (2013). Rax is a selector gene for mediobasal hypothalamic cell types. J. Neurosci. *33*, 259–272.

Manning, L., Ohyama, K., Saeger, B., Hatano, O., Wilson, S.A., Logan, M., and Placzek, M. (2006). Regional morphogenesis in the hypothalamus: a BMP-Tbx2 pathway coordinates fate and proliferation through Shh downregulation. Dev. Cell *11*, 873–885.

Marcos, S., González-Lázaro, M., Beccari, L., Carramolino, L., Martin-Bermejo, M.J., Amarie, O., Mateos-San Martín, D., Torroja, C., Bogdanović, O.,

Doohan, R., et al. (2015). Meis1 coordinates a network of genes implicated in eye development and microphthalmia. Development. *142*, 3009–3020.

Marion, J.-F., Yang, C., Caqueret, A., Boucher, F., and Michaud, J.L. (2005). Sim1 and Sim2 are required for the correct targeting of mammillary body axons. Development. *132*, 5527–5537.

Mathieu, J., Barth, A., Rosa, F.M., Wilson, S.W., and Peyriéras, N. (2002). Distinct and cooperative roles for Nodal and Hedgehog signals during hypothalamic development. Development. *129*, 3055–3065.

Mayer, C., Hafemeister, C., Bandler, R.C., Machold, R., Batista Brito, R., Jaglin, X., Allaway, K., Butler, A., Fishell, G., and Satija, R. (2018). Developmental diversification of cortical inhibitory interneurons. Nature. *555*, 457–462.

Melsted, P., Booeshaghi, A.S., Liu, L., Gao, F., Lu, L., Min, K.H.J., da Veiga Beltrame, E., Hjörleifsson, K.E., Gehring, J., and Pachter, L. (2021). Modular, efficient and constant-memory single-cell RNA-seq preprocessing. Nat. Biotechnol. *39*, 813–818.

Merkle, F.T., Maroof, A., Wataya, T., Sasai, Y., Studer, L., Eggan, K., and Schier, A.F. (2015). Generation of neuropeptidergic hypothalamic neurons from human pluripotent stem cells. Development. *142*, 633–643.

Moir, L., Bochukova, E.G., Dumbell, R., Banks, G., Bains, R.S., Nolan, P.M., Scudamore, C., Simon, M., Watson, K.A., Keogh, J., et al. (2017). Disruption of the homeodomain transcription factor orthopedia homeobox (Otp) is associated with obesity and anxiety. Mol. Metab. *6*, 1419–1428.

Müller, F., Albert, S., Blader, P., Fischer, N., Hallonet, M., and Strähle, U. (2000). Direct action of the nodal-related signal cyclops in induction of sonic hedgehog in the ventral midline of the CNS. Development. *127*, 3889–3897.

Muthu, V., Eachus, H., Ellis, P., Brown, S., and Placzek, M. (2016). Rx3 and Shh direct anisotropic growth and specification in the zebrafish tuberal/anterior hypothalamus. Development. *143*, 2651–2663.

Nagasaki, H., Kodani, Y., and Suga, H. (2015). Induction of hypothalamic neurons from pluripotent stem cells. Interdiscip. Inf. Sci. *21*, 261–266.

Newman, E.A., Wu, D., Taketo, M.M., Zhang, J., and Blackshaw, S. (2018). Canonical Wnt signaling regulates patterning, differentiation and nucleogenesis in mouse hypothalamus and prethalamus. Dev. Biol. *442*, 236–248.

Ohuchi, H., Tomonari, S., Itoh, H., Mikawa, T., and Noji, S. (1999). Identification of chick rax/rx genes with overlapping patterns of expression during early eye and brain development. Mech. Dev. *85*, 193–195.

Ohyama, K., Ellis, P., Kimura, S., and Placzek, M. (2005). Directed differentiation of neural cells to hypothalamic dopaminergic neurons. Development. *132*, 5185–5197.

Padilla, S.L., Carmody, J.S., and Zeltser, L.M. (2010). Pomc-expressing progenitors give rise to antagonistic neuronal populations in hypothalamic feeding circuits. Nat. Med. *16*, 403–405.

Patten, I., Kulesa, P., Shen, M.M., Fraser, S., and Placzek, M. (2003). Distinct modes of floor plate induction in the chick embryo. Development. *130*, 4809–4821.

Pearson, C.A., Ohyama, K., Manning, L., Aghamohammadzadeh, S., Sang, H., and Placzek, M. (2011). FGF-dependent midline-derived progenitor cells in hypothalamic infundibular development. Development. *138*, 2613–2624.

Pera, E.M., and Kessel, M. (1997). Patterning of the chick forebrain anlage by the prechordal plate. Development. *124*, 4153–4162.

Puelles, L. (2019). Survey of midbrain, diencephalon, and hypothalamus neuroanatomic terms whose prosomeric definition conflicts with columnar tradition. Front. Neuroanat. *13*, 20.

Romanov, R.A., Tretiakov, E.O., Kastriti, M.E., Zupancic, M., Häring, M., Korchynska, S., Popadin, K., Benevento, M., Rebernik, P., Lallemend, F., et al. (2020). Molecular design of hypothalamus development. Nature. *582*, 246–252.

Salvatierra, J., Lee, D.A., Zibetti, C., Duran-Moreno, M., Yoo, S., Newman, E.A., Wang, H., Bedont, J.L., de Melo, J., Miranda-Angulo, A.L., et al. (2014). The LIM homeodomain factor Lhx2 is required for hypothalamic tanycyte specification and differentiation. J. Neurosci. *34*, 16809–16820.

Saper, C.B., and Lowell, B.B. (2014). The hypothalamus. Curr. Biol. *24*, R1111–R1116.

Seifinejad, A., Li, S., Mikhail, C., Vassalli, A., Pradervand, S., Arribat, Y., Pezeshgi Modarres, H., Allen, B., John, R.M., Amati, F., et al. (2019). Molecular codes and in vitro generation of hypocretin and melanin concentrating hormone neurons. Proc. Natl. Acad. Sci. U. S. A. *116*, 17061–17070.

Shimogori, T., Lee, D.A., Miranda-Angulo, A., Yang, Y., Wang, H., Jiang, L., Yoshida, A.C., Kataoka, A., Mashiko, H., Avetisyan, M., et al. (2010). A genomic atlas of mouse hypothalamic development. Nat. Neurosci. *13*, 767–775.

Staudt, N., and Houart, C. (2007). The prethalamus is established during gastrulation and influences diencephalic regionalization. PLoS Biol. *5*, e69.

Swaab, D.F. (2003). Human Hypothalamus: Basic and Clinical Aspects, Part I (Elsevier).

Trapnell, C., Cacchiarelli, D., Grimsby, J., Pokharel, P., Li, S., Morse, M., Lennon, N.J., Livak, K.J., Mikkelsen, T.S., and Rinn, J.L. (2014). The dynamics and regulators of cell fate decisions are revealed by pseudotemporal ordering of single cells. Nat. Biotechnol. *32*, 381–386.

Wang, W., and Lufkin, T. (2000). The murine Otp homeobox gene plays an essential role in the specification of neuronal cell lineages in the developing hypothalamus. Dev. Biol. *227*, 432–449.

Wang, L., Egli, D., and Leibel, R.L. (2016). Efficient generation of hypothalamic neurons from human pluripotent stem cells. Curr. Protoc. Hum. Genet. *90*, 21.5.1–21.5.14.

Wolf, F.A., Angerer, P., and Theis, F.J. (2018). SCANPY: large-scale single-cell gene expression data analysis. Genome Biol. *19*, 15.

Xie, Y., and Dorsky, R.I. (2017). Development of the hypothalamus: conservation, modification and innovation. Development. *144*, 1588–1599.

Xu, S., Yang, H., Menon, V., Lemire, A.L., Wang, L., Henry, F.E., Turaga, S.C., and Sternson, S.M. (2020). Behavioral state coding by molecularly defined paraventricular hypothalamic cell type ensembles. Science. *370*, eabb2494.

Yoo, S., Kim, J., Lyu, P., Hoang, T.V., Ma, A., Trinh, V., Dai, W., Jiang, L., Leavey, P., Won, J.-K., et al. (2021). Control of neurogenic competence in mammalian hypothalamic tanycytes. Sci. Adv *7*, eabg3777.

Zhou, X., Zhong, S., Peng, H., Liu, J., Ding, W., Sun, L., Ma, Q., Liu, Z., Chen, R., Wu, Q., et al. (2020). Cellular and molecular properties of neural progenitors in the developing mammalian hypothalamus. Nat. Commun. *11*, 4063.

STAR★METHODS

KEY RESOURCES TABLE

REAGENT or RESOURCE	SOURCE	IDENTIFIER
Antibodies		
Rabbit polyclonal antibody against GNMSELPPYQDTMR peptide from rat/chick Nkx2-1	Ohyama et al., 2005	N/A
Mouse monoclonal antibody against chicken Pax6	Developmental Studies Hybridoma Bank (DSHB)	Cat# Pax6, RRID:AB_528427
Biological samples		
Chicken Hypothalamus samples: dissected from fertilised Bovan Brown eggs	Henry Stewart & Co., Norfolk, UK	N/A
Chemicals, peptides, and recombinant proteins		
Dispase I	Roche	Cat No. 4942086001
Hibernate-E media	BrainBits LLC	Cat No. HE500
Papain	Worthington Chemicals	Cat No. LS003119
B27	ThermoFisher	Cat No. 17504044
GlutaMAX	ThermoFisher	Cat No. 35050061
RNase Inhibitor	Promega	Cat No. N2615
Recombinant Mouse Follistatin 288 (FS-288)	R&D Systems	Cat No. 769-FS-025
Human Follistatin Affinity Purified Polyclonal Ab	R&D Systems	Cat No. AF669
Critical commercial assays		
Chromium Single Cell 3′ Library and Gel Bead Kit v3	10x Genomics	Cat# 1000075
Chromium Single Cell 3′ Chip Kit B	10x Genomics	Cat# 1000073
Chromium i7 Multiplex Kit	10x Genomics	Cat# 120262
Deposited data		
Chicken Raw and analyzed scRNA-Seq data	This paper	GSE171649
Mouse analyzed scRNA-Seq data	(Kim et al., 2020)	GSE132355
Human analyzed scRNA-Seq data	(Zhou et al., 2020)	GSE118487
Experimental models: organisms/strains		
Chicken (Gallus gallus): Fertilised Bovan brown eggs	Henry Stewart & Co., Norfolk, UK	N/A
Oligonucleotides		
Chicken *ARX* custom designed probe set, HCR v3.0	Molecular Instruments, Inc.	XM_025146483.1
Chicken *BMP7* custom designed probe set, HCR v3.0	Molecular Instruments, Inc.	XM_417496.6
Chicken *CA2* custom designed probe set, HCR v3.0	Molecular Instruments, Inc.	NM_205317.1
Chicken *CHRD* custom designed probe set, HCR v3.0	Molecular Instruments, Inc.	NM_204980.2
Chicken *DBX1* custom designed probe set, HCR v3.0	Molecular Instruments, Inc.	NM_001199474.1

(*Continued on next page*)

Continued

REAGENT or RESOURCE	SOURCE	IDENTIFIER
Chicken *DLX1* custom designed probe set, HCR v3.0	Molecular Instruments, Inc.	ENSGALT00000006647.6
Chicken *ELAVL4* custom designed probe set, HCR v3.0	Molecular Instruments, Inc.	NM_204830.1
Chicken *EMX2* custom designed probe set, HCR v3.0	Molecular Instruments, Inc.	XM_025152058.1/ XM_025152057.1
Chicken *FGF10* custom designed probe set, HCR v3.0	Molecular Instruments, Inc.	NM_204696.1
Chicken *FOXA1* custom designed probe set, HCR v3.0	Molecular Instruments, Inc.	XM_004941922.3
Chicken *FOXA2* custom designed probe set, HCR v3.0	Molecular Instruments, Inc.	NM_204770.1
Chicken *FOXG1* custom designed probe set, HCR v3.0	Molecular Instruments, Inc.	NM_205193.1
Chicken *FST* custom designed probe set, HCR v3.0	Molecular Instruments, Inc.	XM_015277250.2
Chicken *HCRT* custom designed probe set, HCR v3.0	Molecular Instruments, Inc.	NM_204185.2
Chicken *HOXB1* custom designed probe set, HCR v3.0	Molecular Instruments, Inc.	NM_001080859.2
Chicken *ISL1* custom designed probe set, HCR v3.0	Molecular Instruments, Inc.	NM_205414.1
Chicken *KRT20* custom designed probe set, HCR v3.0	Molecular Instruments, Inc.	NM_001277981.1
Chicken *LHX9* custom designed probe set, HCR v3.0	Molecular Instruments, Inc.	NM_205426.1
Chicken *MEIS2* custom designed probe set, HCR v3.0	Molecular Instruments, Inc.	XM_015287280.2
Chicken *MSX1* custom designed probe set, HCR v3.0	Molecular Instruments, Inc.	NM_205488.2
Chicken *NEUROG1* custom designed probe set, HCR v3.0	Molecular Instruments, Inc.	NM_204883.1
Chicken *NHLH1* custom designed probe set, HCR v3.0	Molecular Instruments, Inc.	NM_204121.1
Chicken *NKX2-1* custom designed probe set, HCR v3.0	Molecular Instruments, Inc.	NM_204616.1
Chicken *NKX2-2* custom designed probe set, HCR v3.0	Molecular Instruments, Inc.	XM_015283379.2
Chicken *NR5A1* custom designed probe set, HCR v3.0	Molecular Instruments, Inc.	NM_205077.1
Chicken *OLIG2* custom designed probe set, HCR v3.0	Molecular Instruments, Inc.	NM_001031526.1, NC_006088.5|:106522977-106525323 #256 chromosome 1, GRCg6a
Chicken *OTP* custom designed probe set, HCR v3.0	Molecular Instruments, Inc.	ENSGALT00000045360.3
Chicken *PAX6* custom designed probe set, HCR v3.0	Molecular Instruments, Inc.	NM_205066.1
Chicken *PITX2* custom designed probe set, HCR v3.0	Molecular Instruments, Inc.	NM_205010.1/ XM_025149516.1/ XM_025149515.1
Chicken *PROX1* custom designed probe set, HCR v3.0	Molecular Instruments, Inc.	NM_001005616.1
Chicken *RAX* custom designed probe set, HCR v3.0	Molecular Instruments, Inc.	NM_001243724.1

(*Continued on next page*)

Continued

REAGENT or RESOURCE	SOURCE	IDENTIFIER
Chicken *SHH* custom designed probe set, HCR v3.0	Molecular Instruments, Inc.	NM_204821.1
Chicken *SIM1* custom designed probe set, HCR v3.0	Molecular Instruments, Inc.	XM_004940357.3
Chicken *SIX6* custom designed probe set, HCR v3.0	Molecular Instruments, Inc.	NM_204994.1
Chicken *SP8* custom designed probe set, HCR v3.0	Molecular Instruments, Inc.	NM_001198666.1
Chicken *SST* custom designed probe set, HCR v3.0	Molecular Instruments, Inc.	ENSGALG00000007361
Chicken *VAX1* custom designed probe set, HCR v3.0	Molecular Instruments, Inc.	NM_204799.2/ XM_025151484.1
HCR v3.0 amplifier B1, Alexa Fluor-488	Molecular Instruments, Inc.	N/A
HCR v3.0 amplifier B2, Alexa Fluor-488	Molecular Instruments, Inc.	N/A
HCR v3.0 amplifier B3, Alexa Fluor-488	Molecular Instruments, Inc.	N/A
HCR v3.0 amplifier B4, Alexa Fluor-488	Molecular Instruments, Inc.	N/A
HCR v3.0 amplifier B5, Alexa Fluor-488	Molecular Instruments, Inc.	N/A
HCR v3.0 amplifier B1, Alexa Fluor-546	Molecular Instruments, Inc.	N/A
HCR v3.0 amplifier B2, Alexa Fluor-546	Molecular Instruments, Inc.	N/A
HCR v3.0 amplifier B3, Alexa Fluor-546	Molecular Instruments, Inc.	N/A
HCR v3.0 amplifier B4, Alexa Fluor-546	Molecular Instruments, Inc.	N/A
HCR v3.0 amplifier B5, Alexa Fluor-546	Molecular Instruments, Inc.	N/A
HCR Probe Hybridisation Buffer	Molecular Instruments, Inc.	N/A
HCR Probe Wash Buffer	Molecular Instruments, Inc.	N/A
HCR Amplification Buffer	Molecular Instruments, Inc.	N/A
Software and algorithms		
Adobe Photoshop v22.3.0	Adobe Systems	http://www.adobe.com
Adobe Illustrator v25.2.1	Adobe Systems	http://www.adobe.com
CellRanger v.3.10	10x Genomics	http://10xgenomics.com
R v3.6.1	The R project	https://www.r-project.org
Seurat v3.1.5	(Butler et al., 2018)	https://satijalab.org/seurat/
Harmony v1.0	(Korsunsky et al., 2019)	https://github.com/immunogenomics/harmony
Scanpy v1.5.1	(Wolf et al., 2018)	https://scanpy.readthedocs.io/en/stable/
scVelo v0.2.1	(Bergen et al., 2020)	https://scvelo.readthedocs.io/
Monocle v3.0.2	(Trapnell et al., 2014)	https://cole-trapnell-lab.github.io/monocle3/
NicheNet v0.1.0	(Browaeys et al., 2020)	https://github.com/saeyslab/nichenetr
genesorteR v0.4.3	(Ibrahim and Kramann)	https://github.com/mahmoudibrahim/genesorteR
Kallisto v0.46.2	(Melsted et al., 2021)	https://www.kallistobus.tools/
Bustools v2.27.9	(Melsted et al., 2021)	https://www.kallistobus.tools/
Homologene v1.4.68.19.3.27		https://github.com/oganm/homologene

RESOURCE AVAILABILITY

Lead contact

Further information and requests for resources and reagents should be directed to and will be fulfilled by the Lead Contact, Seth Blackshaw (sblack@jhmi.edu).

Materials availability

All unique/stable reagents generated in this study are available from the Lead Contact without restriction.

Data and code availability

- All chick single-cell RNA-seq data have been deposited at GEO and are publicly available as of the date of publication. Accession numbers are listed in the key resources table. All other data reported in this paper will be shared by the lead contact upon request.
- This paper does not report original code.
- Any additional information required to reanalyze the data reported in this work paper is available from the Lead Contact upon request.

EXPERIMENTAL MODEL AND SUBJECT DETAILS

Chick collection

Fertilized Bovan Brown eggs (Henry Stewart & Co., Norfolk, UK) were used for all experiments. Eggs were incubated and staged according to the Hamburger-Hamilton chick staging system (Hamburger and Hamilton, 1992). Briefly, fertilised eggs were stored at 14°C, then incubated in a humidified incubator at 37°C. For all the experiments, both males and females were used. Fertilised eggs were incubated for 28–29 h to obtain HH6, 30–32 h to obtain HH8 (3–5 somite embryos), 40–42 h to obtain HH10 embryos (9–12 somites), 54–60 h to obtain HH 13–15 h, 3 days for HH17/18 and 3.5 days for HH20/21.

All experiments were designed and carried out according to the UK Animals (Scientific Procedures) Act 1986. No ethical approval or Home Office licensing was required, as chicks were not incubated beyond E3.5 (hatching is E21). Named Animal Care and Welfare Officers (NACWOs) had oversight of all incubated eggs.

METHOD DETAILS

Tissue collection

Hamburger-Hamilton stage HH8, HH10, HH13/14, HH15/16, HH18/19, and HH20/21 chick embryos were harvested and neuroectoderm was isolated from underlying mesoderm and endoderm after Dispase I (Cat No. 4942086001, Roche) treatment (Pearson et al., 2011). The following approximate numbers of embryos were dissected, and their cells pooled, for each stage: HH8, 570 (rep 1), 492 (rep 2); HH10, 280; HH13/14, 90; HH15/16, 90; HH18/19, 20 (rep 1), 60 (rep 2); HH20/21, 30. The ventral hypothalamic tissue and small amounts of neighboring tissue were manually dissected at each stage, pooled, and transferred to Hibernate E medium (Cat No. HE500, BrainBits LLC). Tissue was enzymatically digested using Papain (2 mg/mL, Cat No. LS003119, Worthington Chemicals), and cells dissociated into single cells using fire-polished glass pipettes. Papain was neutralized with Hibernate-E medium with B27 and GlutaMAX (Kim et al., 2020). Cells were pelleted at 500 g at 4°C, washed twice in 1 mL cold 1 x PBS, and then resuspended in 200 ul chilled 1 x PBS by gentle pipetting. Cells were then fixed with 800 μL cold 100% methanol as previously described (Alles et al., 2017). Cells were stored at −80°C until scRNA-Seq.

scRNA-seq data generation

Methanol-fixed chick embryos of dissected hypothalamus at HH8, HH8, HH13, HH15/16, HH18/19, HH20/21 were re-hydrated as previously described (Alles et al., 2017). Briefly, cells were washed twice (3000 x g for 5 min at 4°C) and resuspended in RNAse-free PBS with 1% BSA and 0.5 U/ul RNase inhibitor (Cat. N2615, Promega). Cells were then used for the 10x Genomics Chromium Single Cell System (10x Genomics, CA, USA) using V3.0 chemistry per manufacturer's instruction, loading between 8,000 and 12,000 cells per run. Libraries were sequenced on Illumina NextSeq 500 with ~200 million reads per library. Sequenced files were processed through the CellRanger pipeline (v.3.10, 10x Genomics) using the Ensembl *Gallus gallus* genome (GRCg6a, release 95) compiled with the CellRanger *mkref* function.

Explant culture

Explants of prospective hypothalamus were isolated from either HH4 or HH6 embryos by Dispase treatment and cultured in collagen beds (Ohyama et al., 2005). Explants were either treated with recombinant FST (7.5 μg/mL, Cat no. 769-FS-025, R&D Systems) or anti-FST antibody (20 μg/mL, AF669, R&D Systems) for 42 h, and processed for *in situ* hybridization chain reaction (HCR).

In vivo manipulation of follistatin signaling

HH5-6 embryos were injected with 5 μL recombinant FST (7.5 μg/mL) or anti-FST antibody (20 μg/mL) and allowed to develop to HH14 (42 h), and processed for HCR.

Immunohistochemistry

Explants were analyzed by immunohistochemistry according to standard techniques (Manning et al., 2006). Following cryosectioning, the sections were analyzed with the following antibodies: anti-NKX2.1 (1:2000 (Ohyama et al., 2005)) and anti-Pax6 (1:50, DSHB). Secondary antibodies (1:500, Jackson Immunoresearch) were conjugated with Cy3 or FITC.

Chicken HCR

Hamburger & Hamilton stage 8–20 embryos were harvested and fixed in 4% Paraformaldehyde. HCR v3.0 was performed on embryos and cryosections using reagents and modified protocol from Molecular Instruments, Inc. For wholemount HCR, the fixed embryos were dehydrated in a series of methanol and stored at −20°C. The samples were then rehydrated and washed in PBS + 0.1% Tween(PBST). The samples were treated with Proteinase K (10 μg/mL) for 2–3 min, fixed for 20 min and then washed first with PBST, then with 5xSSC. Samples were then preincubated with a hybridization buffer for 30 min. The probe pairs (4–10nM) were then added and incubated at 37°C overnight. For HCR on cryosection, the post-fixed slides were treated with acetylation mix (11.2 μL of Triethanolamine +2.5 μL of acetic anhydride per ml) for 10 min, washed with PBST, fixed again for 10 min and then washed first with PBST, then with 5xSSC.and preincubated with a hybridization buffer for 30 min and the probe pairs (4–10 nM) were added and incubated at 37°C overnight. The next day, samples were washed 4 times in the probe wash buffer, then 2 times in the 5 SSC buffer, and then preincubated in Amplification buffer for 5 min. Even and odd hairpins for each of the genes were snap-cooled by heating at 95°C for 90 s and cooling to RT for 30 min. The hairpins were then added to the amplification buffer and added to the samples and incubated overnight at RT in dark. Samples were then washed in 5x SSC and DAPI was added as a counterstaining.

For multiplexing, after imaging with the first set of probes, the slides were treated with DNAase (0.05 U/μl), washed 3 times in 30% formamide+2x SSC and 3 times in 2xSSC. Slides were then preincubated with the hybridization buffer, the next set of probes were added, and the process was repeated.

Image acquisition

Fluorescent images were taken on a Zeiss Apotome 2 microscope with Axiovision software (Zeiss) or Leica MZ16F microscope or Olympus BX60 with Spot RT software v3.2. Images were acquired using a 4x (Leica), 10x (Leica and Zeiss) and 20× objective (Zeiss). Images were processed using Image-J (FIJI) and Adobe Photoshop 2021. Colocalization analysis was performed using Image-J (FIJI) with Coloc2 and JACoP. Overlap of expression domains was calculated as described (Costes et al., 2004), with Pearson's correlation coefficients (R values) reported. All correlations were statistically significant with Costes' p-value $\geq$0.95.

QUANTIFICATION AND STATISTICAL ANALYSIS

scRNA-seq data analysis

Seurat v3 (Butler et al., 2018) was used to perform analysis following the pipeline described previously (Kim et al., 2020), selecting cells with more than 1000 genes and 1000 UMI, normalized using Seurat *scTransform*, and Harmony (Korsunsky et al., 2019) was used to regress batch effects. Louvain algorithm with a default parameter was used to generate scRNA-Seq clusters, and HCR images across chicken developmental stages and previous hypothalamic scRNA-Seq database HyDD (Kim et al., 2020) were used to identify the spatial location and identity of all hypothalamic-derived clusters in each developmental stage. Extra-hypothalamic clusters were identified when the key gene markers of the cluster were not expressed in HyDD and validated using HCR and by consulting GEISHA (Antin et al., 2014). Differential gene expression tests were performed using Seurat *FindAllMarkers* (LR, regressing depth and cell number variance).

RNA velocity (La Manno et al., 2018) was used to understand the potential developmental trajectory of chicken hypothalamus development and to verify 1) migration of presumptive prethalamus-like cells into the hypothalamus, 2) developmental trajectories of mammillary bodies, PVH/SON, and tuberal hypothalamus. Kallisto and Bustools (Melsted et al., 2021) were used to obtain spliced and unspliced transcripts using –lamanno with GRCg6a chicken genome. Scanpy (Wolf et al., 2018) and scVelo (Bergen et al., 2020) were used to process the Kallisto output with, based on UMAP coordinates obtained from Seurat.

Monocle v3 (Trapnell et al., 2014) was used to perform pseudotime analysis (q value <0.001) to identify differences in gene expression across prethalamus, tuberal, mammillary, and PVN/SON development identified from RNA velocity analysis.

NicheNet (Browaeys et al., 2020) was used to identify receptor-ligand interaction between HH8 and HH10, and HH13 and HH15, assuming that any cluster can be either receiver or sender. First, key genes expressed in the datasets (more than 10% of the population) and background genes were identified. NicheNet ligand activity analysis was then performed by ranking putative ligands and receptors were then inferred from the selected gene lists, with ligand-receptor interaction scores calculated based on a validated ligand-receptor database from NicheNet.

To identify the correlation between chicken, mouse, and human postmitotic hypothalamic neural precursor cells from HH18 and HH20 (this work), E11-E13 mouse scRNA-Seq (Kim et al., 2020), and gestational week 10 human scRNA-Seq (Zhou et al., 2020) were used. Annotation of the human scRNA-Seq dataset was based on a mouse scRNA-Seq database and as shown in the original publication. Seurat *FindIntegrationAnchors* function (default parameter) was used to integrate the 3 datasets after identifying gene homologs across species. Key markers defining individual spatially identified hypothalamic nuclei of the chicken, mouse, and human were then used to plot correlations with genesorteR (Ibrahim and Kramann, 2019).